SHAPING RADIATION CONTOURS WITH A PARABOLIC ACTIVE RECONFIGURABLE ORIGAMI REFLECTOR ANTENNA

A Thesis

by

GREGORY SAMUEL WILSON

Submitted to the Office of Graduate and Professional Studies of
Texas A&M University
in partial fulfillment of the requirements for the degree of

MASTER OF SCIENCE

Chair of Committee,	Darren Hartl
Co-Chair of Committee,	Dimitris Lagoudas
Committee Member,	Robert Nevels
Head of Department,	Rodney Bowersox

August 2020

Major Subject: Aerospace Engineering

ABSTRACT

Origami design allows for the transformation of a flat sheet with discrete face and fold regions into complex three-dimensional shapes. Origami based structures possess desirable engineering features such as compact storage, portability, weight reduction, and reconfigurability. The Active Reconfigurable Origami Reflector Antenna (ARORA) exhibits the aforementioned characteristics of origami structures while incorporating active materials for actuating fold regions. Folds within an origami structure provide intuitively compliant regions for actuation and act as a natural pivot for further folding of the structure. In order to exhibit the utility of the fold regions within origami, ARORA was designed with strategically placed shape memory alloy (SMA) wires in the antenna structure with the goal of morphing its base parabolic shape into a shape that could effectively broadcast to a complex area of coverage via thermal actuation. Numerical simulations using finite element methods are used to investigate actuation strategies of the structure itself while further simulations are utilized to estimate the far-field radiation characteristics. Additionally, the simulations are validated using an ARORA prototype through laser displacement sensing techniques. An efficient global optimization algorithm is then used to explore the ARORA design space and determine the most effective levels of actuation to match a desired broadcast area with a given layout of SMA wires.

CONTRIBUTORS AND FUNDING SOURCES

Contributors

This work was supervised by a thesis committee consisting of my advisor and committee chair, Dr. Darren Hartl, and co-chair Dr. Dimitris Lagoudas of the Aerospace Engineering department along with Dr. Robert Nevels from the Electrical Engineering department at Texas A&M University.

The prototypes shown in Chapter III were fabricated by two undergraduate students within the Aerospace Engineering department, Milton Garza and Collin Invie.

All other work conducted for the thesis was completed by the student independently.

Funding Sources

This work was made possible in part by the National Science Foundation (NSF) under grant number EFRI-1240483. Its contents are solely the responsibility of the authors and do not necessarily represent the official views of the NSF.

DEDICATION

Dedicated to the friends and family that have encouraged me to chase my dreams.

ACKNOWLEDGMENTS

This work would not have been possible without the previous work done by Dr. Sameer Jape and the help of undergraduate students, Milton Garza and Collin Invie.

I would like to thank my fellow graduate students for pushing me to finish this work and being there when motivation was low, particularly Madalyn Mikkelsen and Michayal Matthew. I would also like to acknowledge Glen Colby for being with me all throughout my undergraduate studies and being a great source of competition to strive for excellence against. Finishing my academic career would not have been possible without all of those that stuck with me since the beginning.

NOMENCLATURE

ARORA	Active Reconfigurable Origami Reflector Antenna
BC	Boundary Condition
CONUS	Contiguous United States
DACE	Design and Analysis of Computer Experiments
DIC	Digital Image Correlation
DV	Design Variable
EGO	Efficient Global Optimization
EM	Electromagnetic
FEA	Finite Element Analysis
FE-BI	Finite Element-Boundary Integral
LDS	Laser Displacement Sensor
MoM	Method of Moments
RMSE	Root Mean Squared Error
SMA	Shape Memory Alloy
SMP	Shape Memory Polymer

TABLE OF CONTENTS

Page

LIST OF FIGURES

Page

LIST OF TABLES

Page

CHAPTER I

INTRODUCTION AND LITERATURE REVIEW

Radio signals have been used for years to transmit information between devices and communicate messages to and from groups of people through many forms of wireless devices. Antennas are used to couple a device's electrical current to an electromagnetic (EM) field typically associated with radio waves and signals [1]. Radio waves occupy a relatively large range of the electromagnetic spectrum of light ranging in frequency from roughly 30 Hz to 300 GHz, and these operating frequencies are highly sought after as no two signals can operate on the same frequency within the same area. Due to the directionality of signals and the desire to use as much of the electromagnetic spectrum as possible, antennas have been a widely researched technology and can be designed to function in a vast range of applications. For example, a common whip antenna on a car functions to receive electromagnetic signal from nearly all directions making it useful to receive the same radio station anywhere in a town, while a parabolic reflector dish that one might see on the roof of a house is very directional and only receives signal from one side allowing it to receive strong signals from a known location.

A paraboloid reflects signal back into a circular plane where the strength of signal, or gain, of the antenna is strongest in the center then dissipates radially outward as seen in Figure 1. However, the shape of the reflector needed to reflect a signal into some arbitrary, continuous area is not found simply by tracing the outline of the desired broadcast area and applying signal into that shape. Beam shaping with a single reflector can be seen in

the works of Cherrette et al. utilizing a shaped reflector to establish a far-field pattern close to the shape of the contiguous United States (CONUS) [2]. This research was part of a larger desire to control a single reflector by altering its structure to achieve different signal patterns on demand. Simple corner [3], cylindrical [4,5], or spherical reflectors [6] like those researched by Washington, Gupta, and Yoon et al. could be controlled with piezoelectric actuators to alter the reflector shape. Interest in the field eventually led to more complex antennas being used for beam shaping ranging from origami accordions to cubic antennas [7,8].

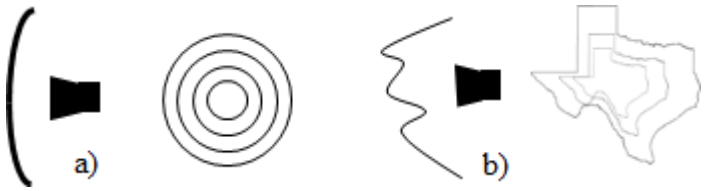

Figure 1a) depicts the ideal broadcast pattern of a parabolic reflector while b) represents a theoretical shaped reflector broadcasting to an arbitrary area

In this work, a highly directional parabolic reflector antenna is going to be studied. The Active Reconfigurable Origami Reflector Antenna (ARORA) is a parabolic reflector that has been discretized into an origami pattern and makes use of the natural pivots, or folds, of origami structures to change the shape of the reflector through shape memory alloy (SMA) actuators from an ideally discretized paraboloid to some other shape. The physical shape change causes the directions that ARORA receives/transmits signal to change and, if controlled properly, allows one to pick and choose a desired directionality of signal. This research will go into structural modeling and validation of the shape change of ARORA along with the coinciding change in broadcast pattern and apply the modeling

methods to an optimization framework that will ascertain the proper actuation techniques to achieve a desired radiation pattern. Several other methods for radiation pattern shaping will be presented throughout this chapter that exemplify other antenna shapes and actuation techniques beyond parabolic reflectors with SMA wires. It can be seen that a variety of antenna shapes can be used to accomplish the goals this research aims to discuss to various degrees of effectiveness and that neither origami nor SMA controlled reflectors are an entirely unique solution to the broadcast shaping problem.

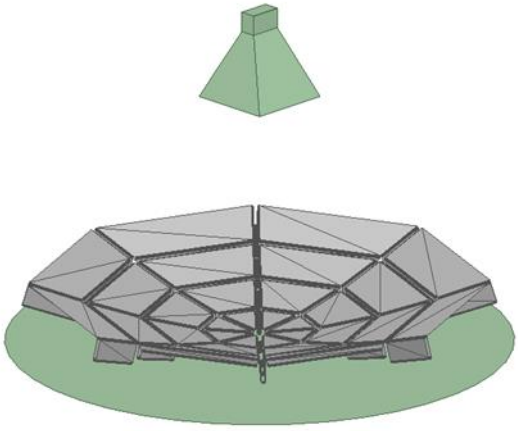

Figure 2: Model of ARORA with a signal horn and reflective backing

Electromagnetic Beam Shaping

Electrically complex array antennas are a well-studied branch of antenna design that use complex interactions of constructive and destructive EM interference of multiple signal feeds in different phases to shape broadcast patterns [1]. A feed in this case is the electrical input or signal given to an antenna either through some sort of alternating current or horn aperture into a reflector. The downside to array antennas is that they can be very electrically complicated and are thus expensive to produce and maintain which has led to

the development and research of single feed reflectors with the capability to have irregular broadcast patterns. One example of which is the reflectarray antenna which uses a pattern of closely spaced, simple electrical elements that could be anything from typical half wave dipole antennas to microstrip patch antennas [9-11]. Another complicated antenna that could be used is a cubic antenna like that used by Sarrazin et. al which can change its radiation contour by changing the properties of a single side of a cube [8]. The desire for less complex reflectors to do increasingly more difficult tasks required stronger solutions to Maxwell's equations for electromagnetism that are only solvable with a large number of approximations and assumptions. Maxwell's equations are a set of coupled partial differential equations that provide the foundation for models of electrical, optical, or radio technologies. Accurate solutions to these equations needed to use the basics of physical optics along with approximations such as the Jacobi-Bessel series like the methods presented by Rahmat-Samii et. al in the 1980's [12].

Techniques to approximate solutions to Maxwell's equations led to the ability to model and predict the behavior of highly irregular single feed reflector antennas that could be created or controlled to broadcast into very complex shapes such as the CONUS [2,5,6]. Naturally, applications of advanced optical methods were not limited to specific uses, but promoted the development of models for reflectors that could change shape to accomplish different goals. For example, Washington and Silverberg used optical methods to model the far-field power outputs of simple variable geometry corner and cylindrical reflectors [13,14]. While these optical methods were strong for their time, the future of EM modeling and antenna design would be shaped by computer power and the potential to solve millions

of equations very quickly with simulation software to solve Maxwell's equations with numerical methods. The advent of more and more ways to model solutions allowed for the introduction of more complicated antenna designs that could incorporate both structural and electromagnetic components, or even control techniques through active materials like piezoelectrics [5,6] or shape memory alloys [15,16].

Shape Memory Alloy Reconfigurable Antennas

SMAs have been used for decades as lightweight actuators due to their ability to change shape due to temperature change or internal stress caused by a force. The material can typically undergo recoverable strains of 5% to 6% purely based on temperature, while specifically crafted metals could potentially go even further beyond under the correct circumstances [17]. SMA wires are simple actuators that are often employed to shrink upon heating thus exerting a force on some structural component causing it to move or deform. This idea can be implemented to simply deflect a beam with a wire attached to the end or alter the curvature composite structures with internal SMA wires [18,19]. A major benefit of using relatively simple SMA actuators such as wires is the ease at which they can be controlled, like in the works of Jayender et. al [20]. The controllability of SMA allows for the actuator to be used for shaping of an antenna's radiation pattern to match very complicated shapes and can be applied to a wide variety of antennas. Parabolic dishes can be morphed to some deformed paraboloid shape using a network of wires [21-24], and helix antennas can be expanded and contracted using wires thus affecting the radiation pattern of the structure [25]. The efficacy of SMA can be amplified even further when coupled with structural design techniques, such as origami, to apply forces and moments

to the already compliant fold regions of a structure and allow for significant shape changes [26,27].

Origami Design for Antennas

The art of origami is primarily used to fold a desired goal shaped into a small area or volume and then unfold the pattern to exhibit large macroscopic shape changes. Common examples of modern origami structures are seen in satellite design which may use origami techniques to conserve volume during launch and unfold once in orbit to reveal solar panels or antennas [28,29]. Origami structures could even be used to alter the thermal properties of a structure [30], simulate grain boundaries within the microstructure of a metal [31], or change an electromagnetic response simply by altering a fold angle [32-36]. Due to the applications of folding, an enormous amount of research has been done on the topic on how to model and predict fold behavior. Tachi designs folded structures by modeling rigid faces in combination with folds that are a combination of an unstable truss and rotation hinge [37], Saito uses a method with elastic or hollow facets which can store some elastic energy for self-deployment [38], and Peraza Hernandez et. al use a method that can account for materials with thickness called “tucked-fold origami” that treats each fold region as a combination of three folds, two convex and one concave [39].Tucked-fold origami discretizes the goal shape into a typical creased fold mesh then removes, or trims, material from the origami mesh in order to add more material meant to compensate for the size of the required tucked-fold. Combining all design techniques for both space applications and morphing along with the capabilities of computer scripting allows for the

optimization of antennas to improve their performance whether that be to match a certain broadcast area or most efficiently amplify their gain.

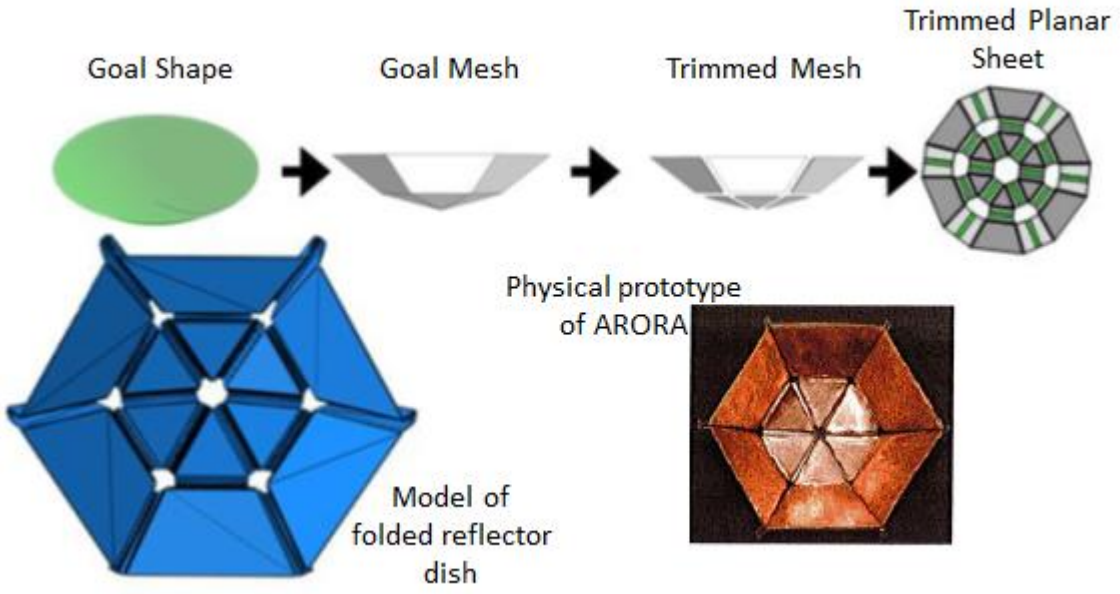

Figure 3: Flow chart of tucked-fold origami design process [39].

Antenna optimization existed prior to the mass availability of computer power but was reserved to finding the optimal dimensions and operating conditions for already well understood types of antennas and antenna arrays as seen in the work by Lo et al. [40]. However, design optimization was made even more practical when computation became widely available and allowed for both structural and electromagnetic analysis to be run simultaneously and create very well designed general use antennas [41-43]. Numerical simulation can now be used for more complicated antennas and coupled with heuristic or numeric optimization algorithms to find optimal designs for reflector shapes, array patterns, variable dielectric materials, bandwidth maximization, or frequency selective surfaces [44-50]. This research hopes to build off of the work of previous antenna

optimization and utilize the techniques of the past while introducing new tools and ideas for future optimization of variable radiation patterns.

CHAPTER II

ENGINEERING TOOLS

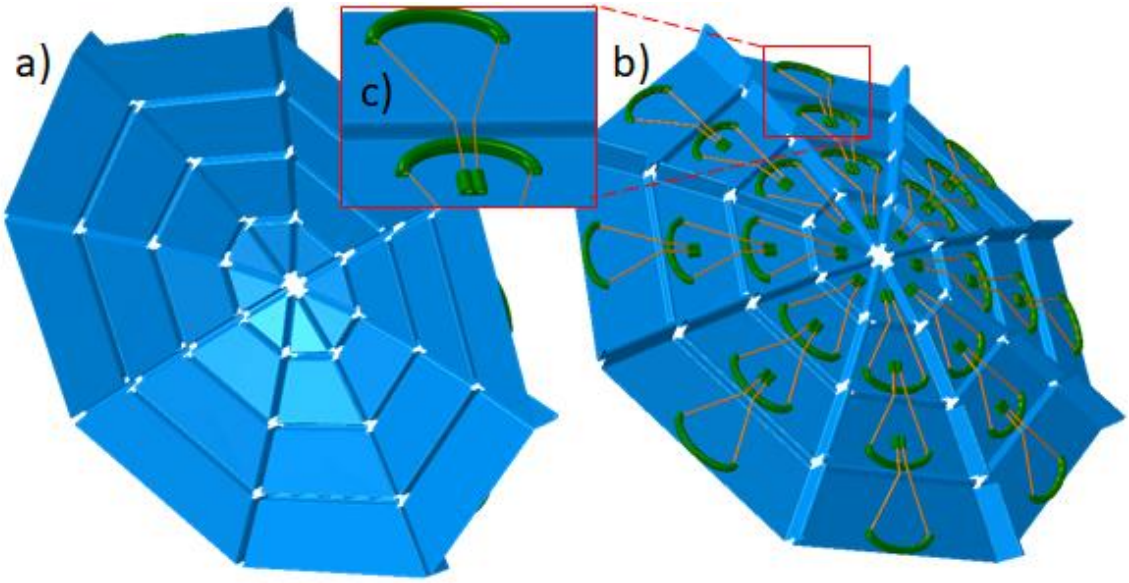

Figure 4a) Front view of the ARORA model b) Back view of model with distinguished wires and wire holders c) Zoomed view of the wire regions on a facet of the discretized antenna

Structural Analysis

The first step in creating the segmented antenna is to design to origami fold pattern that will discretize the parabolic reflector. The finer details of origami design are beyond the scope of this thesis, but more information can be found in the active origami book by Peraza Hernandez et al. [39]. Discretization can be done in several levels based on the desired number of facets in a direction along the paraboloid's circular cross section. This segmentation is denoted as RxC where R is the amount of facets in the radial direction of the cross section and C is the number of facets along the circumferential direction. A

depiction of the R and C directions overlaid on a paraboloid can be seen along with an example of a simple 2x6 segmented antenna in Figure 5.

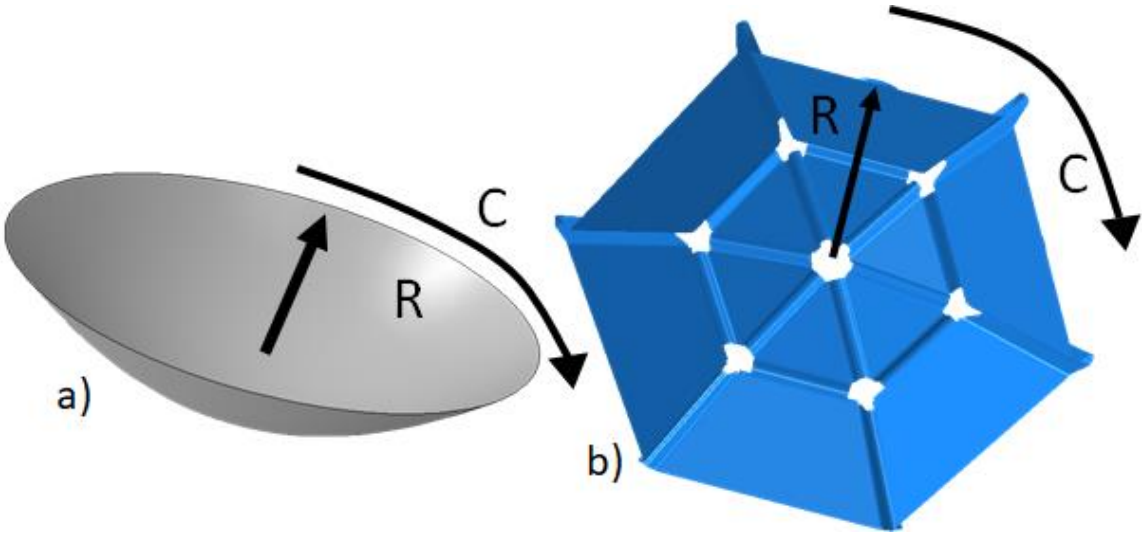

Figure 5a) R and C direction depicted on a typical paraboloid b) an example of a 2(R) x 6(C) ARORA

The origami design codes provided by Peraza Hernandez outputs 3-D models of the antenna like can be made into either physical prototypes or mathematical models for deformation. Creating prototypes for each new design of ARORA would not be economical due to the amount of SMA wire needed for each new prototype and it would be very time consuming to fold a new origami pattern on each iteration. Therefore, finite element analysis (FEA) with a finite element model that can be easily changed is much more ideal for this research. All structural FEA shown for ARORA hereafter is done in Abaqus, a commercial FEA software.

Simply put, FEA works by discretizing a shape into a mesh of elements and solving for the displacements at each of the vertices, or nodes, of the element mesh. These

elements take into account the forces that might be applied to their nodes along with the stiffness that is dependent on their element's shape and material properties. Ultimately, non-linear FEA is about deriving the solution to

$$\underline{F} = \boldsymbol{K}(\underline{u})\underline{u} \tag{1}$$

where $\boldsymbol{K}$ is an NxN matrix of N degrees of freedom, meaning large meshes require the inversion of large matrices to solve for the displacements and rotations of every node, $\underline{u}$, for an applied force, $\underline{F}$. This equation is complicated when nonlinearities from material properties, geometry, or contact are introduced or dynamic responses are needed. For the scope of this research, only geometric and contact nonlinearities will be implemented while the materials will be simply modeled with linear-elastic properties and all analysis will be kept quasi-static. For information detailing the finer intricacies of FEA, it is recommended to read Reddy's book on finite element analysis which outlines much of the theory used by commercial software like Abaqus [51]. The specifics of how the software does its analysis are a trade secret, but it simplifies into a numerical analysis that increments through "time" through the Newton-Raphson method and approximates the displacements of each node for each increment. Time in this case is analogous to the percentage of the force that has been applied for the current analysis step.

The remainder of this section will detail the steps taken in Abaqus to get a functional and coherent model for ARORA. The first step is to assign material properties to the structure. There are only two materials used for this structure, paperboard and polystyrene, which are employed as either 3-layer or 2-layer composites depending on the region of the antenna (e.g. facet, valley fold, mountain fold) as seen in Figure 6.

Paperboard and polystyrene are being used because they are readily available, easy to work with and make physical prototypes out of, and is relatively inexpensive. However, more robust prototypes would most likely be made out of some form of metal to provide the electrical properties desired for ARORA, but that is left for future developments. Polystyrene shrinks upon heating to act as a shape memory polymer (SMP) which motivates the structure to go from a flat origami pattern to the final folded configuration of the antenna. A simple tensile test was performed to determine the linear-elastic properties of both the paperboard and polystyrene for use in the model and future validation of a prototype.

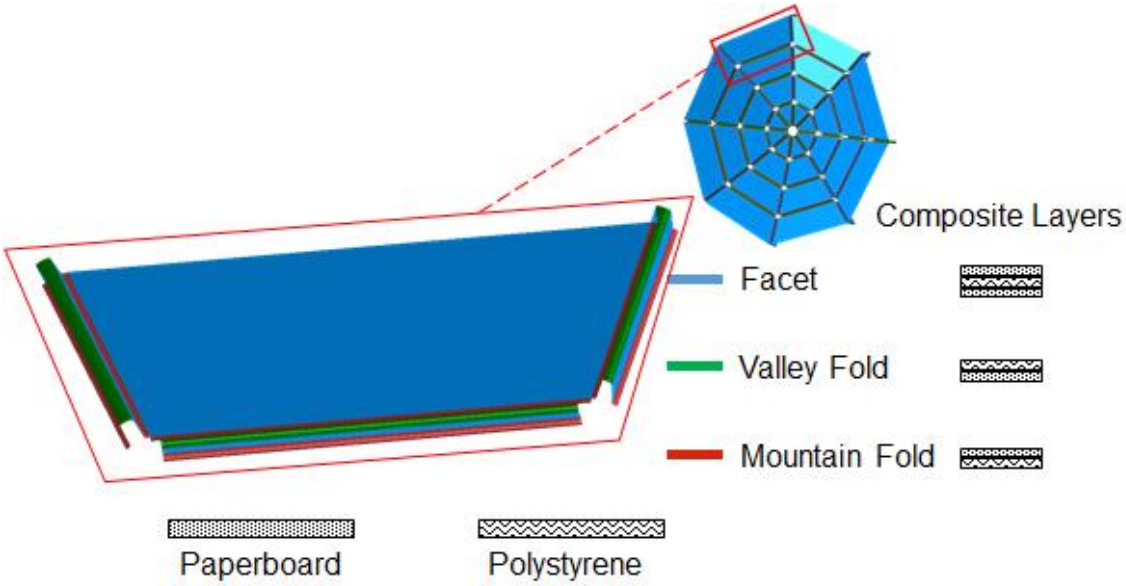

Figure 6: Material assignments for a facet area of ARORA

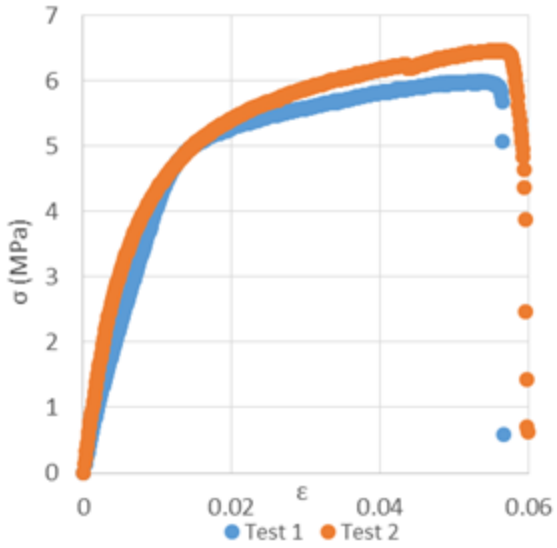

Figure 7: Two separate tensile tests for paperboard cut from the same sample that are used in the model and create the ARORA prototypes shown in Chapter III

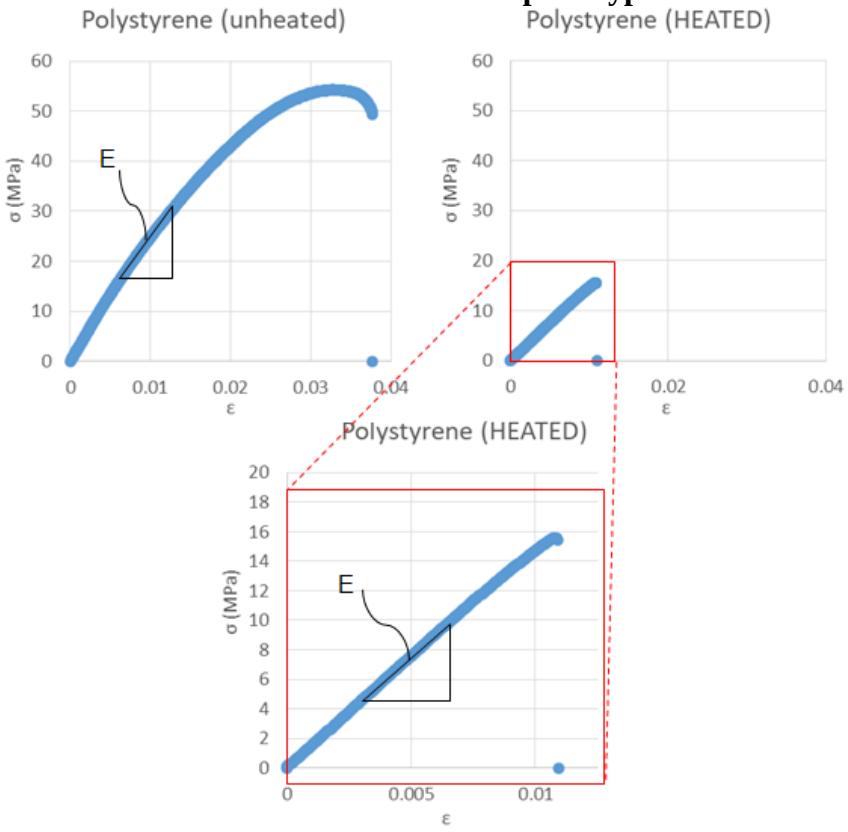

Figure 8: Tensile tests for the two phases of polystyrene in use for the model

Material Name	Elastic Modulus
Paperboard	0.12 GPa (Experimental Average)
Polystyrene	2.5 GPa
Polystyrene – Heated[1]	1.4 GPa
ABS Plastic	17 GPa [52]
NiTi	78 GPa [53]

Table 1: List of material properties in use for the ARORA structural model

Once all material properties have been assigned to the ARORA structure, wires and wire supports/holders can then be placed on the underside of the antenna spanning over each fold in the radial direction. These wires are meant to emulate the shape memory effect of SMA by contracting with an artificially high coefficient of thermal expansion thus exerting a force distributed along the inside of the wire's holder. The forces create moments around the fold regions of the antenna which in turn cause the facets of the segmented structure to rotate about one another. The common form of 1-D transformation of SMA is Hooke's law with extra terms that represent the transformation strain of the material as seen in Eq. (2).

$$\sigma = E[\varepsilon - \varepsilon^t - \alpha(T - T_0)] \tag{2}$$

Where σ is the stress in the material, E is the elastic modulus, ε is the elastic strain, ε^t is the transformation strain, α is the coefficient of thermal expansion, and $(T - T_0)$ is the

[1] The fold regions of ARORA exhibit the heated properties of polystyrene as they are the regions contracting and changing shape during the folding process.

change of temperature from an initial reference. Both E and ε^t can change based on the current phase of the material (what percentage of martensite vs. austenite it is) and the current stress within the material leading to complexities with modeling. α can change with phase, but it is typically such a small change in value that it is often ignored. Hooke's law is still applicable to solve for stress if all inelastic strains are combined into a single representative term and as the intricacies of shape memory alloys are not being researched here, Eq. (1) is simplified to consider an artificial and effective coefficient of thermal expansion, $\hat{\alpha}$ = 0.01 1/˚C, such that $\hat{\alpha}(T - T_0)$ is driven to a maximum value of 2.5% during the course of actuation. Additionally, the elastic modulus of the SMA wire is held constant at a value of 78 GPa which corresponds to the 100% austenitic form of a typical NiTi alloy [52] under the assumption that the final state of the SMA will be closest to heated austenite, but in reality the elastic modulus should vary with the amount actuation strain expected. However, this is complex to model and could be implemented in the future. The stress solved by the FEA software then is the solution to the 1-D modified Hooke's Law equation given in Eq. (3).

$$\sigma = E[\varepsilon - \hat{\alpha}(T - T_0)] \tag{3}$$

The next step in the FEA design process is to define all interactions and contact properties along with defining the type of analysis that will be done. Contact can be a very difficult thing to model mathematically due to the nonlinearities it introduces into the FEA solution. Abaqus offers a few options for contact in order to alleviate some of the convergence difficulties for the numerical approximations needed. First, the penalty method is selected which means that an intersection between one element's nodes to

another element is checked every numerical increment and stiffness is penalized if such an intersection exists. Second, the stiffness penalty of this contact method is reduced because of the harsh penalties that are implemented by default can lead to convergence issues. Finally, the analysis is set to a dynamic, quasi-static analysis rather than a complete static analysis due to the large motions and non-linear nature of the model.

Boundary conditions (BCs) are the last step required to run FEA prior to meshing and beginning analysis. The boundary conditions change depending on the level of discretization of the antenna being analyzed and the purpose of the analysis. However, it always involves fixing all six degrees of freedom for one or more facets as it is a simple boundary condition to replicate for validation. Once the boundary conditions are set it is possible to mesh the model and begin the analysis to observe the effects actuating the SMA wires have on the antenna. Meshing in this case refers to placing nodes at set distances apart from one another on the antenna and creating elements between them so that Abaqus can calculate the stiffness of each element and solve for the displacements of the nodes based on the forces applied by the wire contractions. There are several element types that can be used within the software, but the default linear shell elements will be used for this analysis for simplicity and to lower the computational cost that more complex analysis can have.

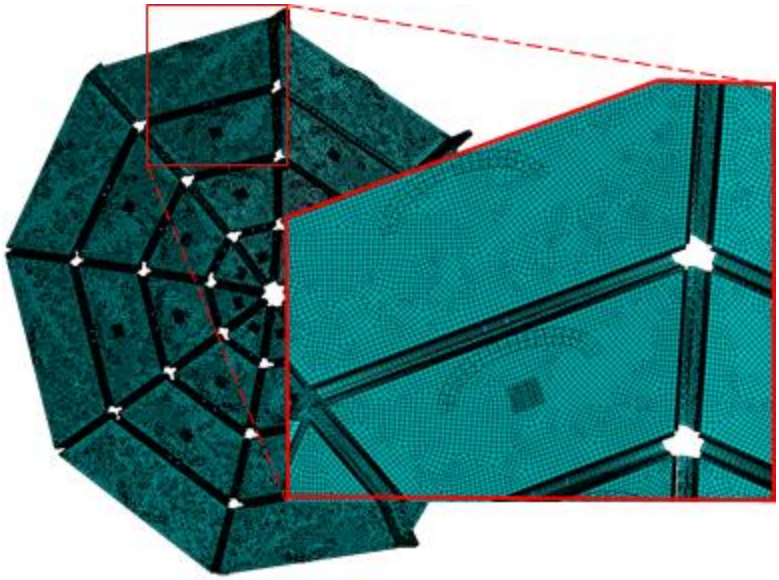

Figure 9: Finely meshed ARORA model

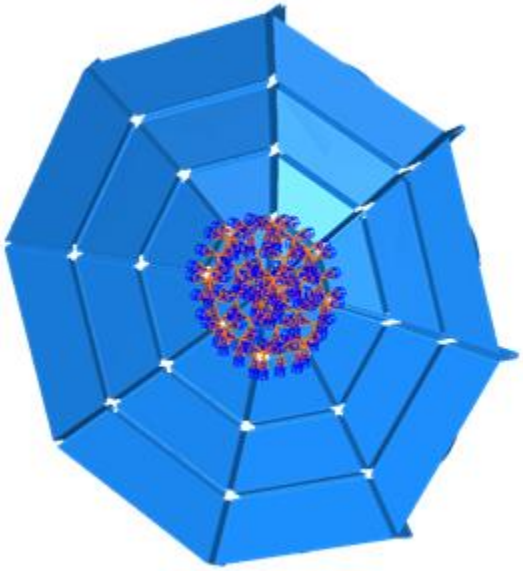

Figure 10: Graphical representation of boundary conditions eliminating all degrees of freedom for the innermost facets of ARORA

Electromagnetic Analysis and Design

Prior to even discretizing a paraboloid and creating a structural model within Abaqus, the antenna itself needs to be designed to have optimal electromagnetic

performance for its expected environment. Parabolic antennas work by reflecting signal radiating from a feed horn placed at the focus of the parabola into a circular shaped plane wave. This type of reflector antenna has one of the highest directivities of a standard and a very narrow beamwidth for its signal, thus allowing it to have a high gain in the direction it is facing. Gain is defined as the ratio of radiation intensity in a given direction and the mean radiation intensity of a perfectly isotropic radiation multiplied by the efficiency of the antenna

$$G(\theta, \varphi) = e\frac{U(\theta,\varphi)}{\bar{U}} \tag{4}$$

where G is the gain, e is the efficiency, U is the radiation intensity in a given direction, and $\bar{U}$ is the mean radiation intensity. It should be noted that gain is typically measured in a logarithmic scale with units of decibels. Works by Jasic and Silver outline the steps to design reflector antennas used in this research and their respective feed horns based on desired operational parameters, but only the basic steps of reflector design will be covered within this research [54,55].

The first step to designing a parabolic dish is to determine what operating parameters are desired. In the case for ARORA, the antenna is envisioned to operate on a satellite with an altitude that could vary from anywhere between low Earth orbit (LEO) to geostationary orbit (GEO) meaning the altitude above the surface of the Earth could range from 1000 km to 35000 km. The varying altitudes make it difficult to decide a desired beamwidth, or angular size of the main signal coming from the antenna, as the beamwidth should depend on the altitude. However, in this case an 8˚ beamwidth was selected as a conservative estimate for the angular size of the contiguous United States at the altitude

ranges for a theoretical satellite. An operating frequency of 10 GHz was selected for the antenna as that is a frequency within the X-Band of frequencies that is commonly used for satellite communications or wireless networks [56]. The final operational parameter needed is to determine the strength of the side lobes, or power in directions other than the main beam (main lobe), which is set as a 30 dB drop from the main lobe to make it a very significant difference in gain between the main and side lobes due to the logarithmic nature of gain measurement.

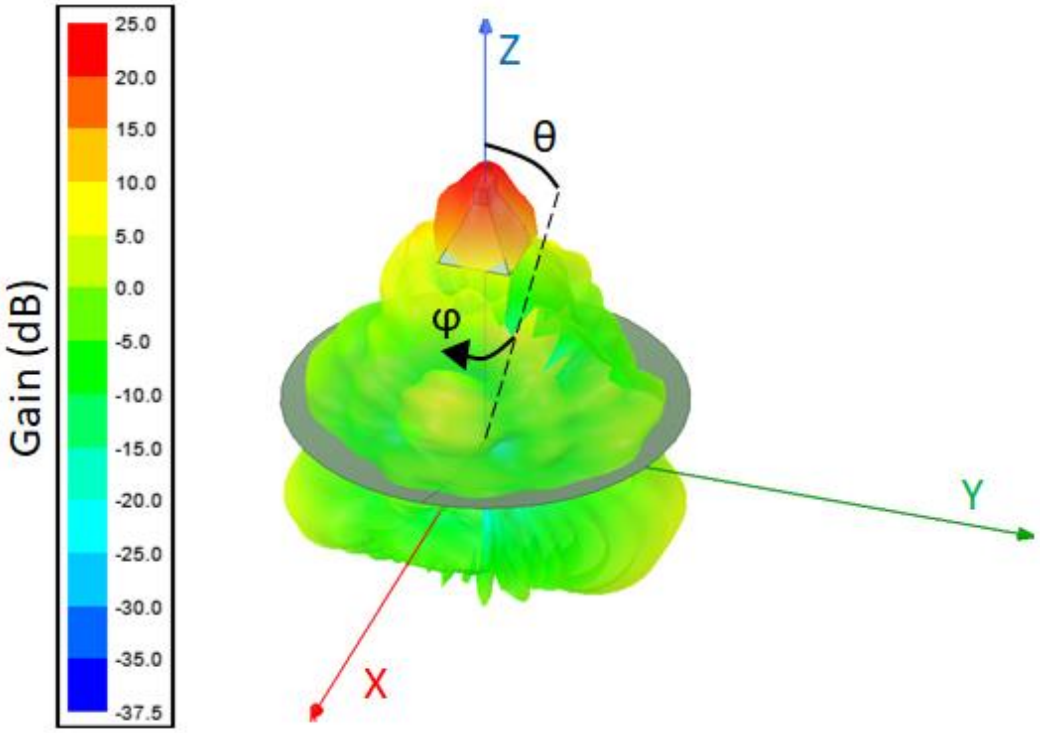

Figure 11: Radiation pattern emanating from an ideal parabolic reflector with the polar angle from the zenith direction, θ, and the associated azimuthal angle, φ, labeled.

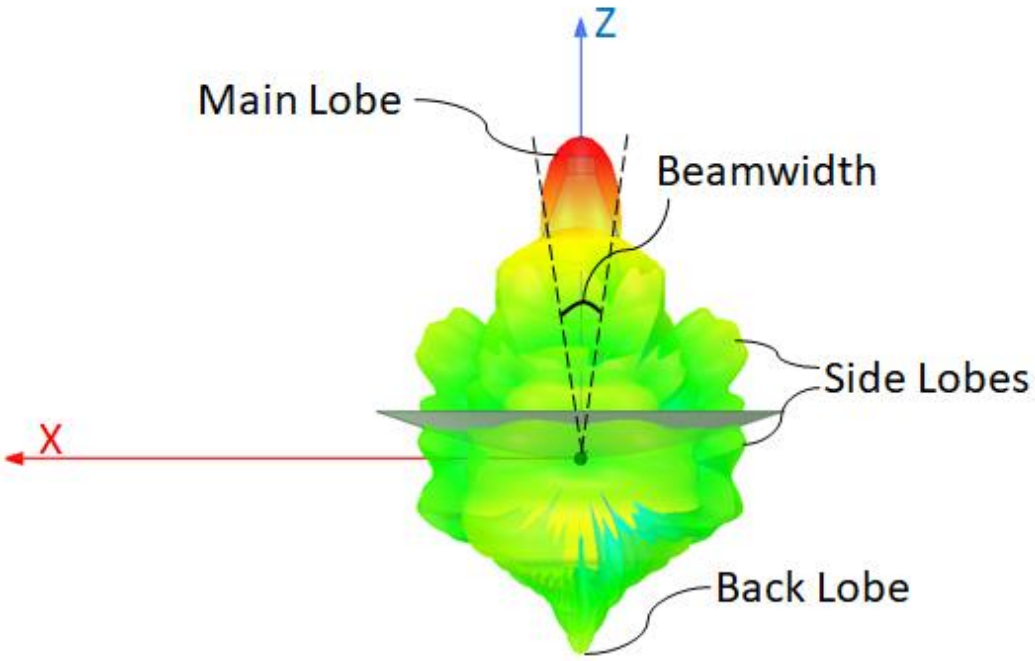

Figure 12: Side view of the radiation pattern of an ideal parabolic antenna with various types of lobes and beamwidth labeled.

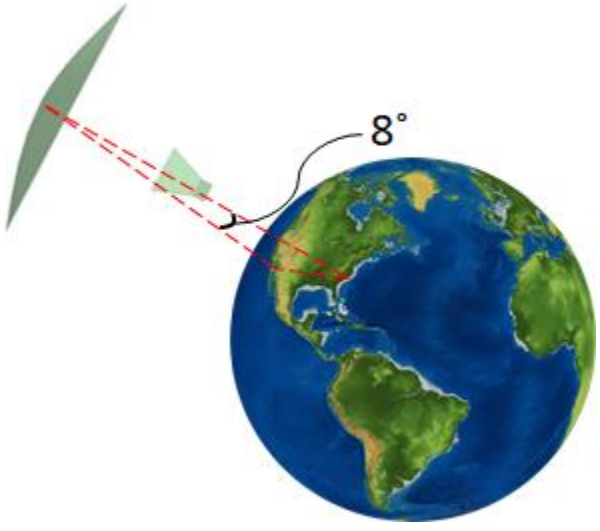

Figure 13: Representation of the beamwidth required to project to CONUS from a geostationary orbit 35000 km above Earth.

Designing the parabolic dish itself can be done in six steps, which are outlined below and utilize methods described by Jasik's Antenna Engineering Handbook [54].

1. Using the desired side lobe level and Figure 12-8 from Jasik, determine the edge taper of the ideal signal horn.
2. From the edge taper found in step 1 and the desired beamwidth, use Jasik Figure 12-6 to determine the ratio of the distance to the focal point to the vertex of the parabola and the diameter of the dish, f/D.
3. Use Eq. (5) BW = 1.27λ/D to calculate the diameter of the antenna where BW is the desired beamwidth in radians and λ is the wavelength for the frequency being used.

$$BW = 1.27\frac{\lambda}{D} \tag{5}$$

4. $f = D\frac{f}{D}$ via a simple proportion.
5. Use geometric relations to find the angle subtended from the focal point to each edge of the parabola, θ_s.

$$\theta_s = 4\tan^{-1}\left(\frac{1}{4\frac{f}{D}}\right) \tag{6}$$

6. Finally calculate how "tall" the parabola needs to be using the geometric relation in Eq. (7)

$$Z_0 = f - \frac{D}{2}\tan\left(\frac{\pi}{2} - \frac{\theta_s}{2}\right) \tag{7}$$

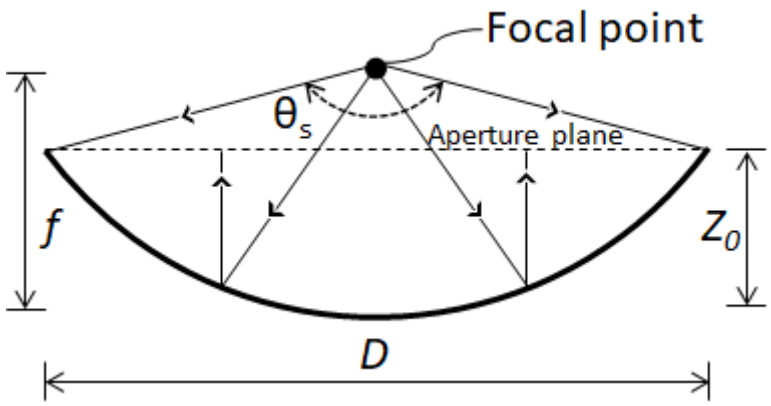

Figure 14: Schematic to show the physical dimensions of a parabolic reflector.

Input design parameters:	Output design parameters:
Frequency = 10 GHz	Edge taper = 14.809 dB
Beamwidth = 8˚	f/D = 0.54422
Side lobe level = 30 dB	D = 272.871 mm
	f = 148.501 mm
	θ_s = 1.7225 rad
	Z_0 = 31.338 mm

Table 2: Input design parameters for the antenna used in this research with its associated output design parameters needed for the final design model.

Solving for the gain of the antenna in every θ and φ direction is tedious to do by hand, and there are no simple analytical solutions for the complex shape of ARORA, so the computational electromagnetic modeling software, ANSYS HFSS, was used to solve for the radiation pattern of the antenna. Several material properties and electromagnetic solution conditions need to be set similarly to the Abaqus setup discussed previously. To

begin, the parabolic reflector is imported into ANSYS and a simple feed horn is placed at its focal point. In this case, the horn was modeled after a small feed horn that was available in the Texas A&M Electrical Engineering department to allow for any future validation of the modeled antenna and given the properties for a perfect electrical conductor (PEC). The facets of ARORA, or the entire paraboloid when modeling a non-origami antenna, were given the conductive properties of copper ($5.8x10^7$ S/m) because faces of the fabricated prototypes of ARORA could easily be covered in a copper tape for validation. The fold regions of the antenna, however, were given a non-conductive material property (1 S/m) as they cannot easily be covered in a copper tape.

The solution methods used for this analysis are important to consider for both the accuracy of the calculated radiation pattern and computational cost of each analysis. ANSYS HFSS has several methodologies to within its options to change how the numerical analysis is conducted, but only the options used in this research will be discussed. It would be possible to solve the entire problem with a large, spherical radiation boundary surrounding the antenna/horn system using a full-wave finite element method, but it is more cost effective to change the boundaries for each individual component [57,58]. The horn region is surrounded by an air box with a Finite Element-Boundary Integral (FE-BI). FE-BI combines finite element methods and the method of moments (MoM) for EM problems with complex geometries and various materials. All surfaces of the antenna, conductive or not, are assigned an integral equation (IE) region which uses the MoM to solve for EM fields formulated as integral equations for electrically large antennas ($D \sim 10\lambda$) [58,59]. Running the analysis with the listed material properties and

boundary conditions with a frequency of 10 GHz yields the gain in all directions from the antenna.

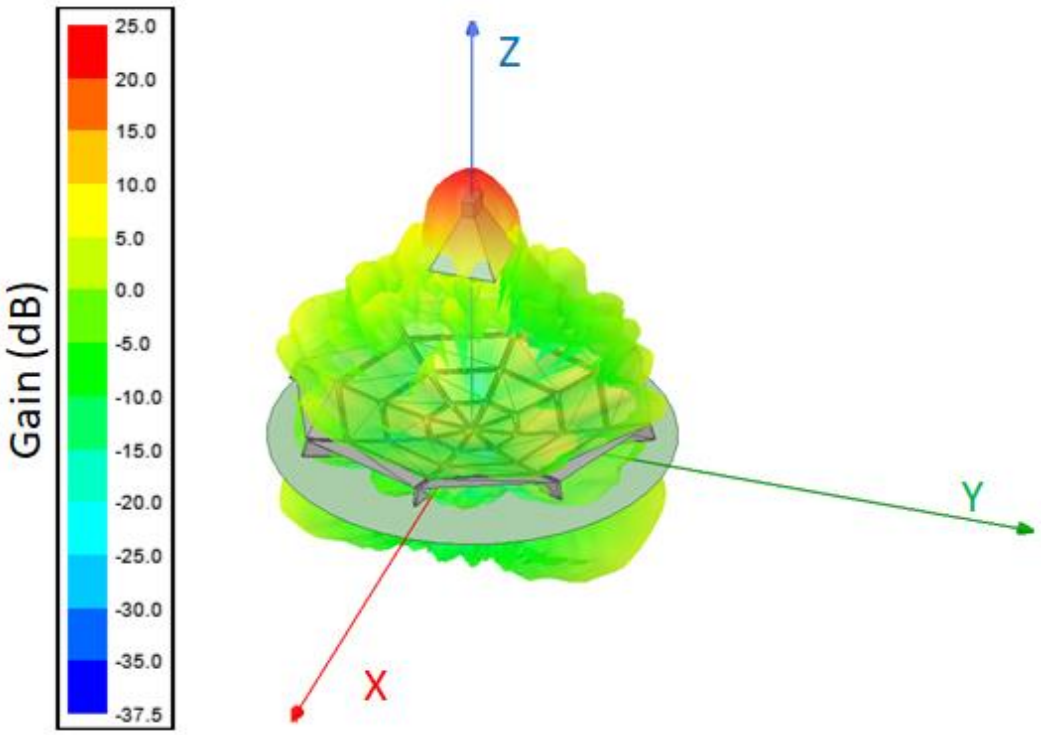

Figure 15: Signal pattern from an undeformed 4x8 ARORA.

Global Optimization

Many optimization algorithms exist for the purpose of finding the optimum of highly non-linear systems, and several studies have been conducted comparing the current state-of-the-art heuristic algorithms [60, 61]. However, the major downside of these methods is the large amount of designs that must be tested in order to find global optima with some cases of a particle swarm algorithm requiring 400,000 total designs to converge to a solution for complex systems. A design in this context refers to a k-dimensional vector of variables that can be changed within a problem. More mathematical approaches to

optimization like that seen in gradient-based optimization methods cannot be used in the case for ARORA due to the absence of known gradients in the design space [62]. Each design tested corresponds to a calculation, experiment, and/or test that must be carried out which, depending on the complexity, could take a very long time. One design alone could take upwards of 30 minutes to complete in the case of the structural and electromagnetic finite element analysis for ARORA. It is therefore necessary to use novel optimization techniques that can reduce the total number of designs needed to be analyzed for expensive problems. This is the problem Efficient Global Optimization (EGO) aims to solve. The EGO algorithm was created specifically for the purpose of optimizing problems that have time consuming black-box functions [63]. The following section will explain how the algorithm works to effectively reduce the time needed for optimization while not compromising accuracy of the final solution.

EGO is based on one core assumption: that the function it is trying to optimize is a continuous one. This means that for any design points, **x**, in k dimensions, that are close together, the function values evaluated at those points, y, should be similar values. A common and simple way to estimate how y is related to x for continuous functions is to use the linear regression formula

$$y\left(\mathbf{x}^{(i)}\right) = \sum_{h=1}^{k}[\beta_h f_h\left(\mathbf{x}^{(i)}\right)] + \epsilon(\mathbf{x}^{(i)}) \quad (8)$$

$$(i = 1, \dots, n)$$

where the superscript, (i), represents the i-th tested point out of n points in the design space, β_h is an estimated coefficient, f_h is a linear or non-linear function of $\mathbf{x}$, and ϵ is the error in y associated with each $\mathbf{x}^{(i)}$.

The question that should arise when understanding the implications of Eq. (8) is how one determines if two points are "close." One could intuitively consider the Euclidian distance between points that weights the distances in all dimensions the same way. However, this would fail to capture the importance of some design variables (DVs) compared to others. To demonstrate this, imagine that a farmer were to try to design an enclosure for a farm to maximize the amount of space for their animals while not crossing into their neighbor's property. The farmer might consider the amount of fence they have along with the terrain, shape of their property, and positions of trees. The trees do not have much impact on the amount of usable area for a relatively open field and therefore should not be considered as heavily in the optimization problem as the other variables. However, if this problem were modeled using typical linear regression it would consider the trees as equally contributing to the complexity of the problem. This is an untrue statement and would lead to an inefficiency in modeling.

A different way to approximate y($\mathbf{x}$) besides simple linear regression with Euclidian distance must be considered to efficiently model complex design spaces, and this is why a stochastic process model called the Design and Analysis of Computer Experiments (DACE) [64] is used as the foundation of the EGO algorithm. DACE is comprised of two key equations that are ultimately used to express Eq. (8) in a simpler way. First, DACE determines how close design points are based on the relative importance

of each design variable, θ_h, and relative smoothness of the estimated function in direction h, p_h, leading to

$$d\left(\mathbf{x}^{(i)}, \mathbf{x}^{(j)}\right) = \sum_{h=1}^{k} \theta_h |x_h^{(i)} - x_h^{(j)}|^{p_h} \quad (9)$$

where $d(\mathbf{x}^{(i)},\mathbf{x}^{(j)})$ is the non-Euclidian distance used between the i-th and j-th points. This distance is used to evaluate the correlations between every point (i, j).

$$\mathrm{Corr}[\epsilon(\mathbf{x}^{(i)}), \epsilon(\mathbf{x}^{(j)})] = \exp[-d\left(\mathbf{x}^{(i)}, \mathbf{x}^{(j)}\right)] \quad (10)$$

$$(\theta_h \geq 0,\ p_h \in [1,2])$$

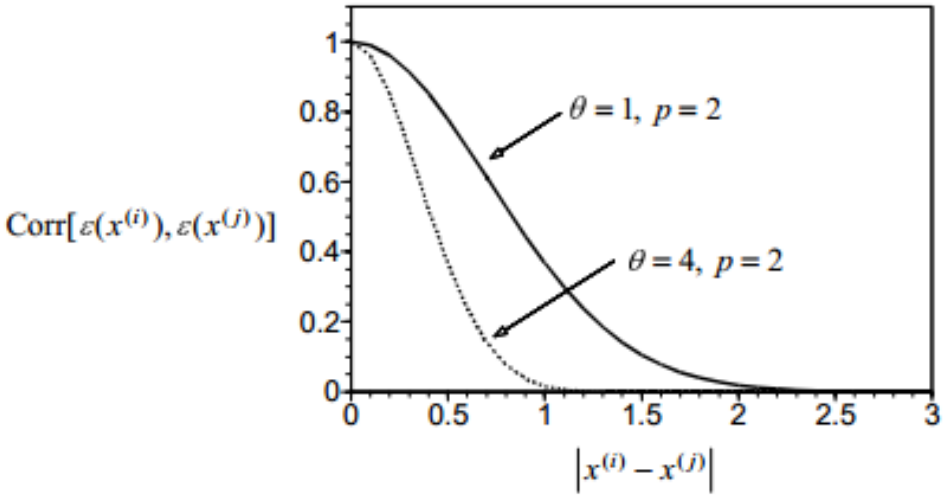

Figure 16 Graph showing how correlation between designs is affected by the difference and relative importance of design variables. Note how high importance can lead to low correlations even for similar designs. Reprinted with permission from [63].

Defining the error term, ϵ, as Normal(0, σ^2) where σ^2 is the standard deviation between all tested **x** it is then possible to couple Eq. (9) and Eq. (10) into a new linear regression model

$$y\left(\mathbf{x}^{(i)}\right) = \mu + \epsilon(\mathbf{x}^{(i)}) \quad (11)$$

where μ is the mean of all y points. Eq. (11) is a powerful equation because it does not need to consider the functional behavior or regression coefficients of **x**. The equation simply needs to consider the error between the function values of any tested point and the model's prediction of that same point calculated from correlations. The DACE model can therefore be expressed using 2k+2 parameters which would be μ, σ^2, θ_1, …, θ_k, p_1, …, p_k. The underlying issue in DACE at this point is that if one knew all of the θ_h and p_h values for all **x** points then there would be no need to model the data set as a function because one could easily find an optimal design if so much was known about the effects of $\mathbf{x}^{(i)}$ on $y^{(i)}$. It is then necessary to maximize the likelihood, or trust, in the model presented.

$$\frac{1}{(2\pi)^{\frac{n}{2}}(\sigma^2)^{\frac{n}{2}}|\mathbf{R}|^{\frac{1}{2}}}\exp\left[-\frac{(\mathbf{y}-\mathbf{1}\mu)'\mathbf{R}^{-1}(\mathbf{y}-\mathbf{1}\mu)}{2\sigma^2}\right] \tag{12}$$

y in this case represents the vector of each $y(\mathbf{x}^{(i)})$ and **1** is an n-vector of ones. The likelihood function Eq. (12) only introduces one new variable that has yet to be considered: the n x n matrix, **R**. However, **R** is not entirely a new variable as it is a matrix with entries (i, j) that are the values of Eq. (9) and thus relates the mean and standard deviation of the set of designs back to the correlations between each individual design. As these values of μ and σ^2 are not exactly known, one needs to solve Eq. (12) for the estimated values $\hat{\mu}$ and $\hat{\sigma}^2$ (variables denoted $(\hat{\cdot})$ will refer to their estimated values for the rest of this section).

$$\hat{\mu} = \frac{\mathbf{1}'\mathbf{R}^{-1}\mathbf{y}}{\mathbf{1}'\mathbf{R}^{-1}\mathbf{1}} \tag{13}$$

$$\hat{\sigma}^2 = \frac{(\mathbf{y}-\mathbf{1}\hat{\mu})'\mathbf{R}^{-1}(\mathbf{y}-\mathbf{1}\hat{\mu})}{n} \tag{14}$$

Substituting Eq. (13) and Eq. (14) into Eq. (12) yields the likelihood function that must be maximized to obtain all $\hat{\theta}_h$ and $\hat{p}_h$ values.

Thus far all that has been discussed is fitting a model that can predict function values at points where the function value is already known. This is helpful in its own ways, but does not necessarily find optima that are not located at an already tested point. It is therefore necessary to begin predicting the function values for unknown points and strategically adding points until there is little error between tested and estimated function values. The first part of this new problem can be solved by approximating the error between the actual function values for a new test point, $\mathbf{x}^*$, and the estimated value of that point based on all current values in the DACE model $\hat{y}(\mathbf{x}^*)$. Based on the continuity of the model and statement made previously, the error for predicted points should be very small near tested points and relatively large far from test points.

When adding a new point, $\mathbf{x}^*$, one must consider the effect that point will have on values such as $\hat{\mu}$ because adding any point to a sample could change the sample's mean or standard deviation. To do this, let $\mathbf{r}$ be an n-vector of the correlations between the error terms of $\mathbf{x}^*$ and all currently sampled points such that the i-th element of $\mathbf{r}$ can be defined by $r_i \equiv \text{Corr}[\epsilon(\mathbf{x}^*), \epsilon(\mathbf{x}^*)]$. This leads to a new version of Eq. (11) where the error term is replaced with a term representing a predicted error based on correlations and the current estimated average of the data set.

$$\hat{y}(\mathbf{x}^*) = \hat{\mu} + \mathbf{r}'\mathbf{R}^{-1}(\mathbf{y} - \mathbf{1}\hat{\mu}) \tag{15}$$

An important observation of Eq. (15) is that when the function value of an already sampled point of the set, $\mathbf{x}^{(i)}$, is predicted using the equation, its true function value, $y^{(i)}$, is obtained which corresponds to no error in prediction.

$$r_i(\mathbf{x}^{(i)}) \equiv \mathrm{Corr}[\epsilon(\mathbf{x}^{(i)}), \epsilon(\mathbf{x}^{(i)})] = \mathbf{R}_i$$

$$\mathbf{r}'\mathbf{R}^{-1} = \mathbf{R}_i'\mathbf{R}^{-1} = (\mathbf{R}^{-1}\mathbf{R}_i)' = \mathbf{e}_i'$$

$$\hat{y}\left(\mathbf{x}^{(i)}\right) = \hat{\mu} + \mathbf{e}_i'(\mathbf{y} - \mathbf{1}\hat{\mu}) = \hat{\mu} + \left(y^{(i)} - \hat{\mu}\right) = y^{(i)} \tag{16}$$

This gives way to using the mean squared error of the prediction, denoted by $s^2(\mathbf{x}^*)$, as the measure for error in the model's prediction of new points because that error metric suggests there will should no error in prediction at sampled points while the root mean squared error (RMSE), s, will be roughly σ at points that are far away from previously sampled designs.

$$s^2(\mathbf{x}^*) = \sigma^2\left[1 - \mathbf{r}'\mathbf{R}^{-1}\mathbf{r} + \frac{(1-\mathbf{1}'\mathbf{R}^{-1}\mathbf{r})^2}{\mathbf{1}'\mathbf{R}^{-1}\mathbf{1}}\right] \tag{17}$$

Finally, once the error of a new point can be determined, it is possible to compute what design will be the next best design to test. For the case of trying to minimize an objective value, this is done by considering the current minimum of all tested designs, f_{min}, and finding the expected improvement that a new point, $\mathbf{x}^*$, will yield. Expected improvement, $E[I(\mathbf{x}^{(i)})]$, depends on the distribution function of all currently sampled points, Φ(.), along with a standard normal distribution of function values, ϕ(.). In simpler terms, the expected improvement of a new point will be a compromise between choosing points that are near local minima and points that have a high chance of having error. Points are added until there is no longer an expected improvement above a desired improvement

value, at which point the global optimum is considered to be found and the EGO algorithm can stop.

$$E[I(\mathbf{x})] = (f_{min} - \hat{y}(\mathbf{x}))\Phi\left(\frac{f_{min} - \hat{y}(\mathbf{x})}{s(\mathbf{x})}\right) + s(\mathbf{x})\phi\left(\frac{f_{min} - \hat{y}(\mathbf{x})}{s(\mathbf{x})}\right) \quad (18)$$

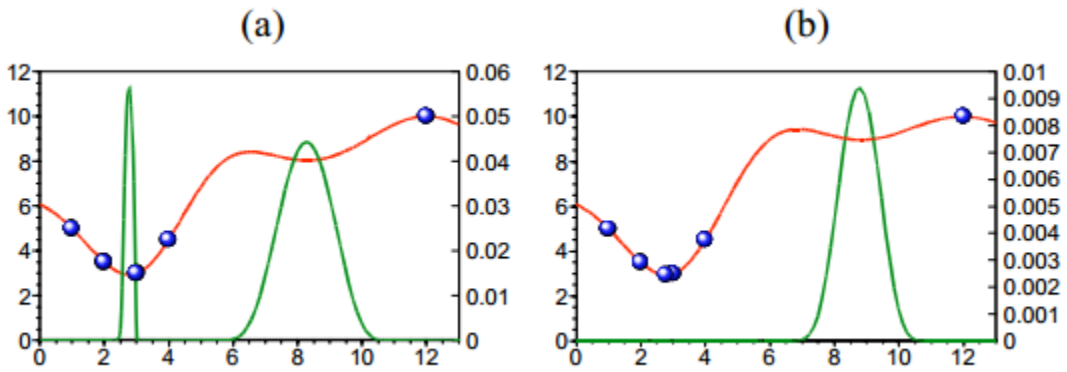

Figure 17 The red line represents a 1-D DACE predicted function while the green line represents an expected improvement to find a better minimum at any x value. (a) Initial calculations for 5 points in a sample (b) New functions after the optimal 6th point is added. Reprinted with permission from [63].

Non-Intrusive Displacement Measurements

Validation of the structural deformation of the antenna was done using a Laser Displacement Sensor (LDS). LDS was implemented as an alternative to more complicated 3-Dimensional Digital Image Correlation (DIC) due to the difficulty of capturing out of plane deformations with that technique. The system used to track the deformation of ARORA throughout actuation utilizes a Keyence IL-600 laser displacement sensor like that shown in Figure 18 and the rotation about a fixed axis with a Vishay Rotary Potentiometer. Scans of ARORA are taken before and after the heating of SMA wire to compare shape the centerline of the antenna in both states. The combined system of the sensory and potentiometer allow for the distance and angle measured from the origin of

the laser with respect to a fixed rotating axis. With that information collected, the (x, y) coordinates of a measurable surface of object can be measured with respect to the point of rotation. To determine radial distance from the LDS, the Keyence IL-600 boasts variable sampling rates (100, 250, 500, 1000, 3000 Hz) and a high resolution measurement (0.05 mm) at relatively large distances (200 – 1000 mm). This sensor is ideal for this research as it is non-intrusive and will not alter the structural properties of the antenna itself. A Vishay Model 357 Rotary Potentiometer is used to determine the LDS position while attached to a rotational shaft. As shaft is rotated relative to the main sensor body, an output voltage signal varies linearly with its rotation angle.

Figure 18: Keyence IL-600 Laser Displacement Sensor

The main shaft of the laser system is a threaded 4 mm steel rod allowing for washer and nut, coupling rotation between the laser system and the rotary shaft. The shaft is braced at two points by a bearing block harness to eliminate the possibility for out of plane

rotation. The potentiometer, fixed by a structural support, is connected directly to the threaded rod by a 6 mm to 4 mm shaft coupler, locking the rotation between the laser sensory and potentiometer. Then, the bearing block and potentiometer support are connected separately to a fixed base. In total, the LDS measures about 3” W x 6” H x 16” L, providing a compact lightweight design for quick installation and test preparation. Rotation of the LDS is controlled via an attached 12""lever arm allowing for a smoot, manually controlled rotation of the sensor. During each measurement, the LDS scans an ARORA prototype from the outer most edge radially inward towards the center of the antenna.

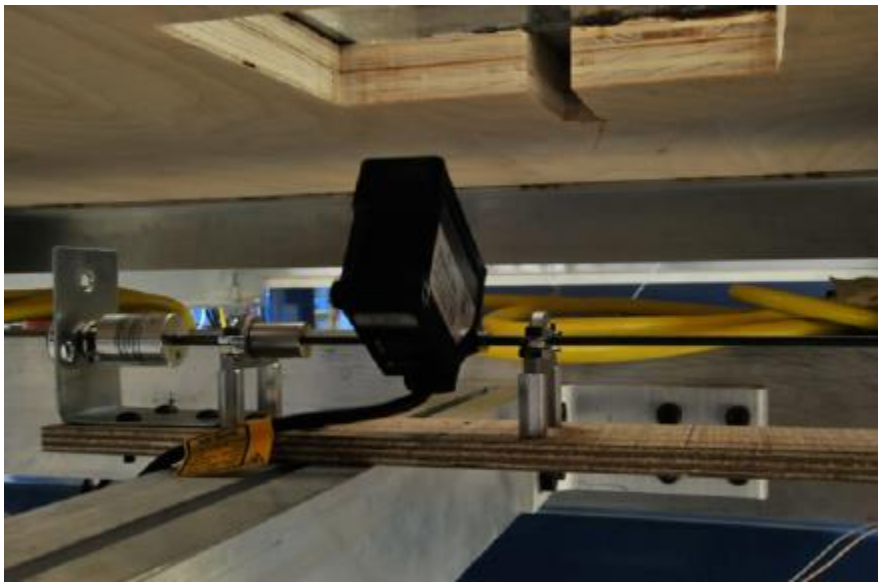

Figure 19: Laser Displacement Sensor mounted beneath the ARORA prototype

CHAPTER III

RESULTS AND ANALYSIS

This chapter will detail the results of structural finite element analysis of generic and simple actuation cases of ARORA along with some of the changes and simplifications used during the structural modeling process. Then, the electromagnetic impacts of the deformation of the antenna will be explored. Finally, there will be a discussion on the experimental validation of ARORA via a physical prototype.

Finite Element Analysis and Results

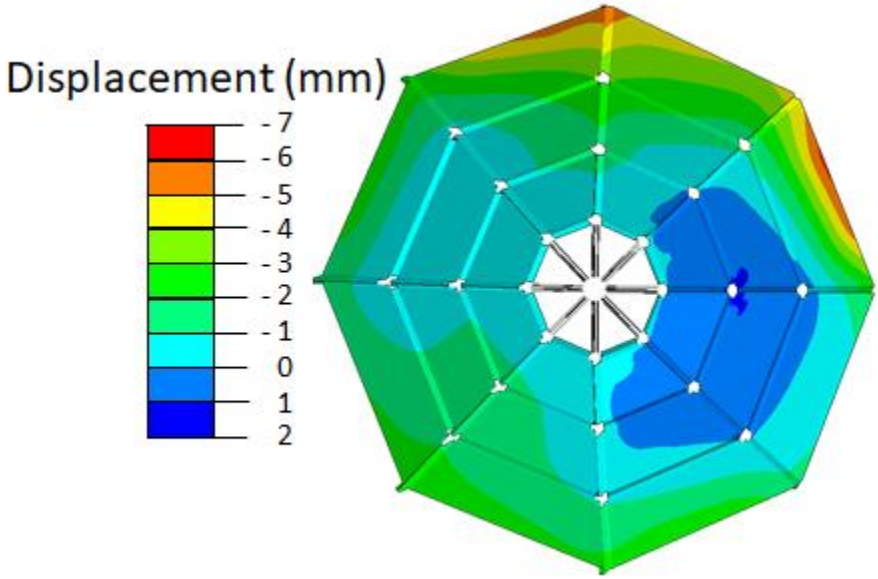

Figure 20: Example output of FEA for the final ARORA model. Displacement is measured from the zenith direction

The results and runtime of FEA can be highly sensitive to changes in the inputs to the analysis. This section will discuss the methods done to help reduce the computational cost of FEA while converging to the same achieved solution. However, due to the design

study carried out for this research, only the methods used 4x8 ARORA FEA will be discussed in detail.

Run times for numerical analysis with finite elements are primarily influenced by the mesh size, or the number of elements used to discretize the structure. Abaqus and many other commercial finite element software allow the user to alter the amount of nodes or elements, select element types, and modify the general complexity of the mesh used to discretize the model being analyzed. The element type influences the number of nodes in each element, and the degrees of freedom that must be solved for by inverting the stiffness matrix is directly related to the number of nodes. In simple terms, if one wants to analyze a structure quickly they should use the smallest number of simple elements as possible, but not so few elements as to bias the accuracy of the solution. It is for this reason that a mesh convergence study was carried out on the ARORA model in order to reduce the number of elements used for each numerical analysis. The most significant tactics used for computational cost reduction came from both the reduction of element slice per circumferential discretized “slice” of the antenna and changes to the creation of the model itself.

Beyond simply reducing the element sizes used to mesh the structure, another element reduction tactic done for ARORA was removing the inner facets of the antenna. Those facets are unable to move and contribute little to the analysis due to their boundary condition that fixes all six degrees of freedom of the elements that comprise those eight facets. Therefore, the inner facets can be removed for the structural analysis and added back to the antenna during post processing as nothing about their shape will change during

the deformation of the SMA wires. Instead, the boundary condition that was placed on the inner faces is transferred to the underside of the wire holders that were attached to the facets as they shared degrees of freedom thus making it an equivalent boundary condition for the antenna. It should be noted that the tucked fold regions connecting the inner-most faces were mostly removed as the boundary condition on the facets prevented them from affecting the analysis as well. The only parts of the tucked fold region that were kept serve as necessary geometric properties for the initial setup of the model and are comprised of one completely fixed element each to make their effect on the runtime negligible.

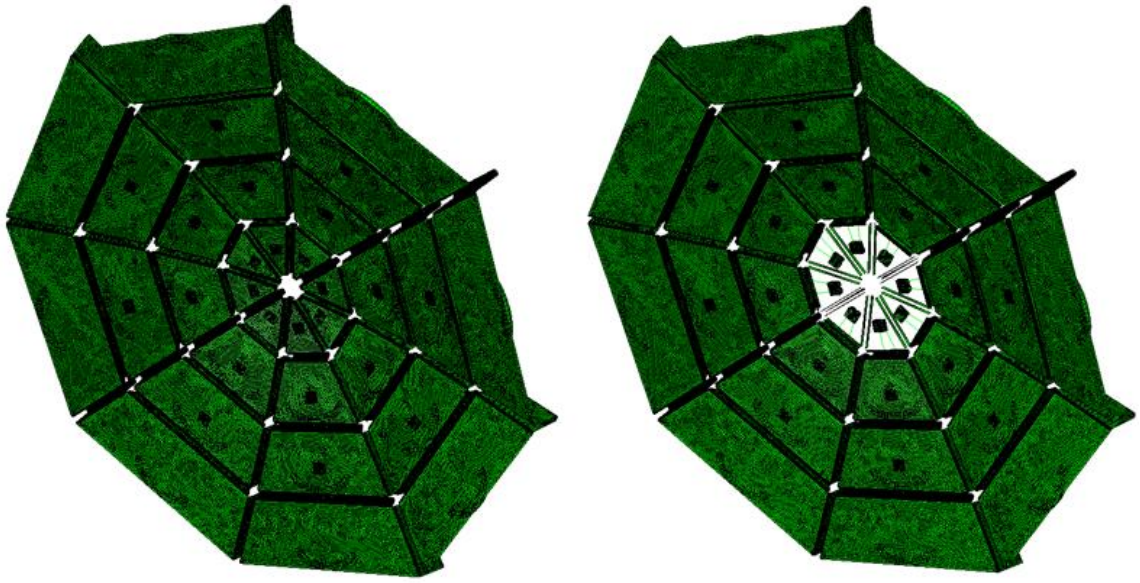

Figure 21: A picture of the fully meshed ARORA with and without inner faces

The final strategy used to minimize the run time for the FEA run in this research was to change the contact properties between the SMA wires and their respective holders and fold regions. Abaqus has two methods to determine if a node is in contact with an element, and one of such methods is much more accurate but computationally expensive

than the other. This more accurate method is called the finite sliding method. In this contact method, the normals between one element's nodes and another's is calculated for each time increment throughout the analysis. These calculations start to significantly contribute to the overall runtime of the FEA when many increments are needed for the analysis to converge to a solution which is the case with ARORA. The other method, small sliding, only calculates these normal vectors at the beginning of the analysis and uses those same vectors throughout every increment regardless of how much they may have changed. The initial models of ARORA had finite sliding for every contact region in the model as that should be the most accurate contact method in any given situation. Small sliding was then implemented in the model in the hopes of reducing run time which it did, but it also led to an error in which the wires would slip out of their holders due to the large deformations of the antenna causing displacements too large for the original normals to maintain contact. For these reasons a combination of finite and small sliding was used in the final ARORA model in which finite sliding was used for the wire holders and small sliding was used for the tucked fold region. The run time study can be seen in the table below.

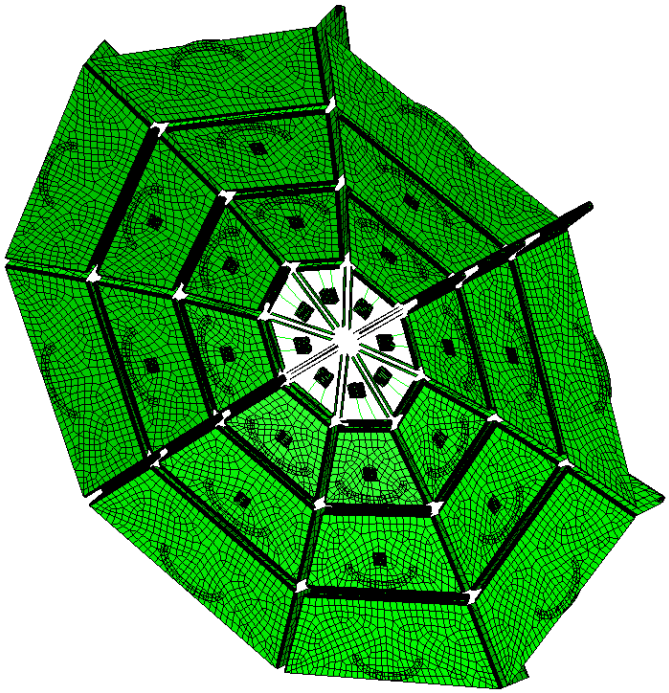

Figure 22: Coarse ARORA mesh without inner faces

Inner Faces	# Elements/slice	Sliding Type	Max Deflection	Run Time
Yes	26845	Finite	35.02°	3 h 25 m
No	24689	Finite	35.05°	3 h 4 m
No	24689	Small	20.59°	1 h 15 m
No	24689	Combination	34.34°	1 h 47 m
No	6402	Combination	35.60°	0 h 34 m
No	6402	Small, No Separation	N/A	1 h 30 m +

Table 3: Comparison of computational time for various FEA settings

Once the model for ARORA has been finalized it is then possible to perform a study on the overall behavior of the antenna to determine what wires might have the largest effects on the structural deformation of the antenna. To do this, a study on a single discretized slice was carried out by actuating combinations of the three SMA wires on the slice and observing the effect each wire has. The three wires underwent a 2.5% strain if

they were being used in the current analysis and the deformations caused, measured in degrees rotated from the cross-sectional plane of the antenna can be seen in Figure 23. It appears that the inner most wire, wire 1, has the most significant influence on the deformation of the structure as the rotation of the inner faces can propagate out to the outer faces. Additionally, since the inner faces are smaller they have less inertia for the dynamic analysis so an equivalent force on a smaller face should have a greater impact than that of a larger face. An important observation of this study is the evident warping of the faces due to the forces of the wires, which is especially visible when wire 3 is in use. The center of the facet has a region that is clearly undergoing a larger rotation than the rest of the face implying that there is a significant deformation caused by the forces that would not be seen if the faces were rigid and only undergoing a rigid body motion. This warping phenomenon will be explored further in the validation section of this chapter. It should further be noted that the inner most triangular facet provides nothing for the analysis and does not rotate due to its fixed boundary condition discussed previously in this section and is excluded when running analysis for the whole antenna.

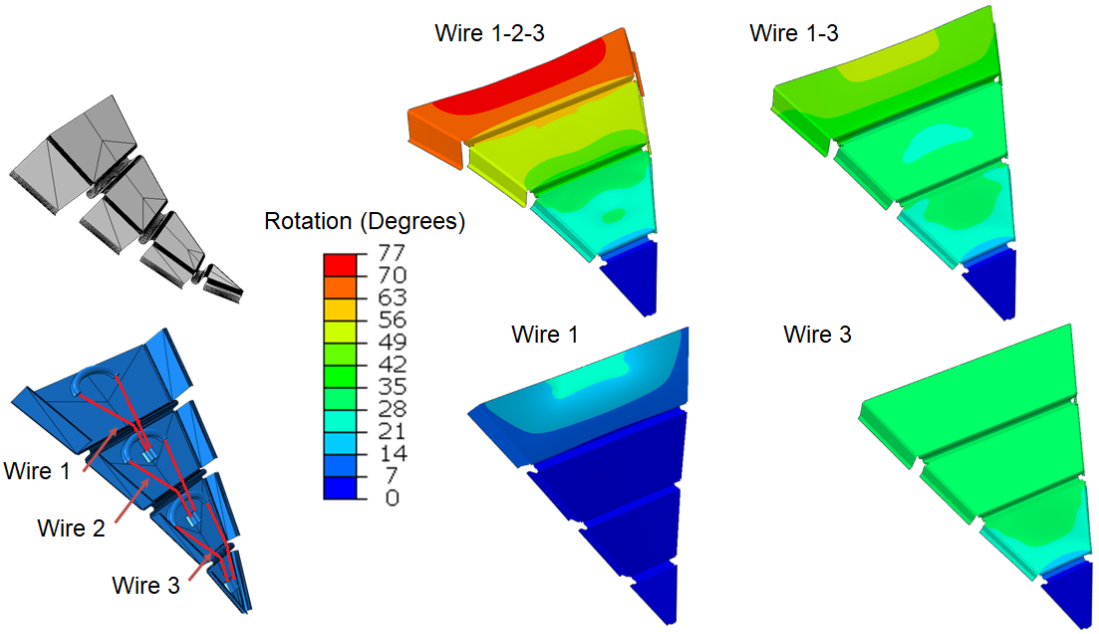

Figure 23: Exploration of the effects each wire has on the deformation of a single slice. Rotation is measured from the aperture plane of the antenna.

Electromagnetic Results

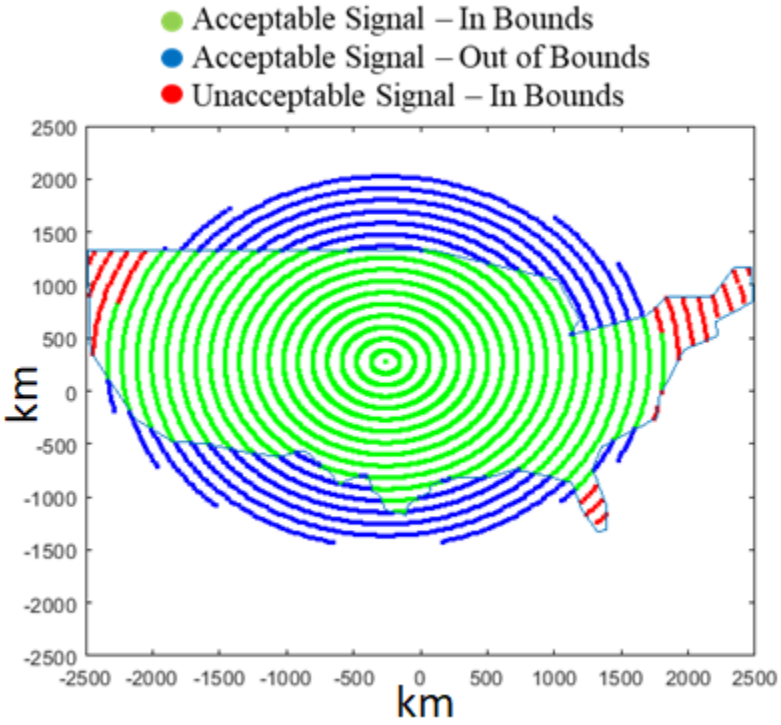

Figure 24: Example projection of an ideal parabolic reflector's radiation pattern onto the shape of CONUS

The purpose of ARORA is to match its signal to a shape so the first step to analyzing the effectiveness of the antenna is to project its signal onto a desired shape. The signal itself is influenced by the deformation of the antenna, but how well that signal matches is impacted by not only the radiation pattern but also its orientation and origin point of the signal. Assumptions made prior to the signal projection were that the goal shape was flat (i.e. the curvature of the Earth is not being considered) and that the antenna is pointing directly at the centroid of the goal shape. A library of countries around the world was created using the latitudes and longitudes of discrete points along the border of

the country and those positions were converted onto a Cartesian plane. The centroid point (C_x, C_y) of the country could then be calculated using the method outlined in Eq. (19-21) which calculated the centroid for an n-1 sided polygon comprised of n points.

$$C_x = \frac{1}{6A}\sum_{i=0}^{n-1}(x_i + x_{i+1})\,(x_i y_{i+1} - x_{i+1} y_i) \tag{19}$$

$$C_y = \frac{1}{6A}\sum_{i=0}^{n-1}(y_i + y_{i+1})\,(x_i y_{i+1} - x_{i+1} y_i) \tag{20}$$

$$A = \frac{1}{2}\sum_{i=0}^{n-1}(x_i y_{i+1} - x_{i+1} y_i) \tag{21}$$

Where x_i and y_i are the x-coordinates and y-coordinates, respectively, for the i^{th} point of the polygon and A is its area.

After the centroid of the goal shape has been calculated, the antenna is then placed at a desired altitude above that point (25000 km in the case of CONUS) and the gain given in spherical coordinates $G(\theta, \varphi)$ is projected onto the flat shape. The gain for a specific point within the shape can be found by extending the rays emanating from the antenna in angles θ and φ, such that the point in Cartesian coordinates on the two-dimensional plane, $\mathbb{D}$, can be found. Given points $\boldsymbol{p} \in \mathbb{D}$, where $\mathbb{D}$ is a two-dimensional domain of all computed results that contains a propagation target subdomain of interest, $\mathbb{C}$, (i.e. $\mathbb{C} \subset \mathbb{D}$) an indicator function, $I(\boldsymbol{p})$, can be introduced.

$$I(\boldsymbol{p}) = \begin{cases} 1, & \boldsymbol{p} \in \mathbb{C} \\ 0, & \boldsymbol{p} \notin \mathbb{C} \end{cases} \tag{22}$$

The design goal is to then minimize both the area in $\mathbb{D}$ outside of $\mathbb{C}$ that is receiving too strong of a signal and the area within $\mathbb{C}$ that is receiving too weak of a signal. This can be done by defining a threshold value of gain, G_t, which is set to 3 dB less than the maximum gain value of the antenna. 3 dB is used as it corresponds to the half-power of the antenna

signal and every point receiving less than half of the maximum amount of signal may be considered out of the broadcast area. Employing the Heaviside function:

$$H(x) = \begin{cases} 1, & x \geq 0 \\ 0, & x < 0 \end{cases}$$

the full objective function to minimize, $\hat{f}$, can then be expressed as Eq. (23).

$$\hat{f} = \int_D \left[I(\boldsymbol{p}) H\big(G_t - G(\boldsymbol{p})\big) + \big(1 - I(\boldsymbol{p})\big) H(G(\boldsymbol{p}) - G_t) \right] dA \qquad (23)$$

However, as HFSS computes gains, $G(\boldsymbol{p})$, along discrete rays originating from the reflector in spherical coordinates for θ in increments of 0.25˚ from 0˚ to 180˚ and φ for every 1˚ from 0˚ to 360˚. The points $\boldsymbol{p}(\theta_i,\varphi_j) \in \mathbb{D}$ thus represent the intersections of these rays with $\mathbb{D}$. Given such a discrete field of output gain in spherical coordinates, (θ_i, φ_j), the discretized objective function taking into account the number of discretized points in θ, N_θ, the number of discretized points in φ, N_φ, and transformation of $\boldsymbol{p}$ into $p_{ij} = \boldsymbol{p}(\theta_i, \varphi_j)$ is Eq. (24).

$$f = \sum_{i=1}^{N_\theta} \sum_{j=1}^{N_\varphi} \left[I(p_{ij}) H\left(G_t - G(p_{ij})\right) + \left(1 - I(p_{ij})\right) H\big(G(p_{ij}) - G_t\big) \right] = b + r \qquad (24)$$

Where b represents the number of discrete points within $\mathbb{D}$ but outside of $\mathbb{C}$ that are receiving sufficient gain and r represents points within $\mathbb{C}$ receiving inadequate signal. Points that contribute to b and r are represented by blue and red points, respectively, in figures such as Figure 24. If the stress within any of the SMA wires exceeds a yield stress, σ_y, of 650 MPa associated with a reasonable yield stress of NiTi in its austenitic form [53], a penalty value of 2000 is added to the objective function for that set of design variables to signify their infeasibility creating the final objective function Eq. (25). 2000 was chosen as a penalty value because there are approximately 2000 discretized points within the

shapes used for this research so the penalty effectively doubles the objective score. Even larger penalties could have been used, but a penalty of 2000 effectively makes any stress infeasible design worse than any feasible design. Additionally, *b* and *r* could be weighted to place more importance on one aspect of the objective score over another, but both are considered equally important to minimize for the purpose of this research.

$$f = b + r + 2000H(\sigma - \sigma_y) \tag{25}$$

Enigneering Design Study

Exporting the deformed shape from Abaqus into ANSYS can prove difficult due to the complex shapes created from deformation and can lead to problems in completing the analysis. Therefore, it was necessary to simplify what was imported into ANSYS so that the modeling and solution process within the software could go without error. A study was performed in order to discover the simplifications to the model that could be implemented that involved changing how the antenna itself was imported and what parts of the antenna were used for analysis. The antenna was initially being exported from Abaqus and then imported as a .stl file which discretizes geometry into a mesh completely comprised of triangles and is mainly used for 3D printing, but it is possible to export the geometry as a .sat file which offers a much more robust representation of the geometry with the purpose for modeling. The .stl antennas behaved very strangely due to the very small, but present, voids between each connected face which lead to complicated and unphysical results. An additional factor that adds to modeling difficulty is the tucked-fold regions of the origami structure, so comparisons between the electromagnetic performance

of antennas with and without the fold regions were also conducted. The removal of tucked-fold regions may seem like an egregious change in the model, but since the fold regions were given non-conductive properties in the model it should follow that they would not contribute much to the analysis regardless of if they are included or not. However, the tucked-fold regions could be simplified by manually filling the gaps between facets with a simple rectangle to act as a pseudo-fold region given non-conductive properties, but this is difficult to script given the changing geometry of the antenna when it is undergoing deformation so it is only presented here as an option that may be beneficial to include in the future for all ARORA models. In the end, a method of importing the antenna via .sat files and using no fold regions was selected as it has the closest performance to the ideal parabolic reflector and is the easiest to implement.

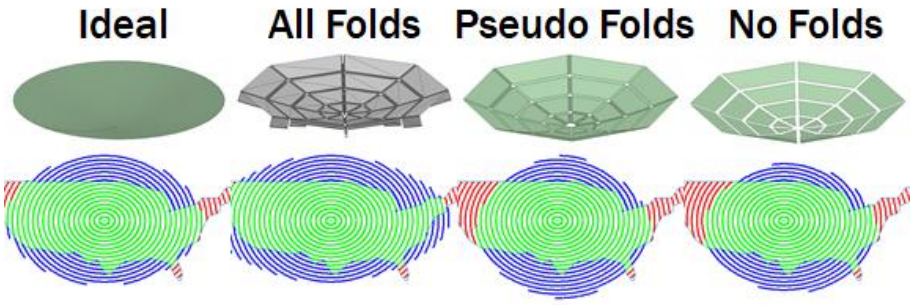

Figure 25: Projection of various signal patterns onto CONUS

Antenna Type	File type	Maximum Gain	Objective Score
Ideal parabolic reflector	.sat	23.7	1481
ARORA with all folds	.stl	21.6	1735
ARORA with pseudo-folds	.sat + ANSYS	21.7	1664
ARORA with no folds	.sat	22.3	1486

Table 4: Relevant outputs for differing antenna models

No wires on the underside of ARORA have been modeled within ANSYS thus far because of their difficulty to import and assign thickness and properties. It is believed that the wires are going to be coated in both a thermally and electrically insulating coating so their effect on the overall radiation pattern would be negligible. Signal is being reflected from the conductive surfaces on the front side of the antenna which were given the properties of copper and could theoretically carry a surface current around to the back side of the antenna and transfer to one of the wires spanning the non-conductive fold regions of ARORA. This is not an issue based on one of the fundamental theorems of electromagnetics, the reciprocity theorem, which states that a radiator in close proximity to a reflector has little to no effect on the surface currents of the reflector thus a negligible impact on its far-field radiation pattern [65, 66]. Moreover, one could consider the wires to be acting as "random wire antennas" on the underside of the structure changing the overall radiation pattern. These types of antennas exhibit about 10 dB of gain at most in the direction of their main lobe, which is significantly less than the typical 20 dB gain of ARORA [67]. The contributions of those random wire antennas will not be considered in this work, but could possibly be used in future work towards developing a more robust antenna model.

The overall behavior of the electromagnetic response to the structural deformation of the antenna should be studied prior to designing an antenna to match a specific shape in order to determine if the deformation has an effect on radiation pattern. Interpretation of which wires are being actuated for ARORA can be difficult to represent, but the

actuation configuration for the antenna can be visualized by a figure like that seen in Figure 26. There are 24 wires attached to the underside of the antenna and each of the 24 sections of the doughnut chart seen in Figure 26 represent one of those wires spanning each facet of the antenna such that the sections most radially outward represent the external most wires and so on. While the discretization of ARORA here is 4x8, there are not four radial discretizations in the figure as the inner most faces do not have any wire that could cause that face to deform. Each section of the figure is colored from a darker shade, where the darkest shade means that wire is undergoing 100% actuation (of the 2.5% strain possible), and a completely white shade means that wire is not in use at all. In the case of Figure 26, only one circumferential slice is being actuated by the greatest amount possible to explore the effect of how a single slice influences signal pattern.

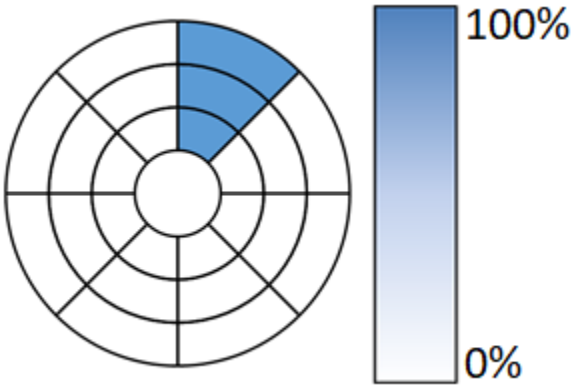

Figure 26: Graphical representation of input actuation levels for ARORA

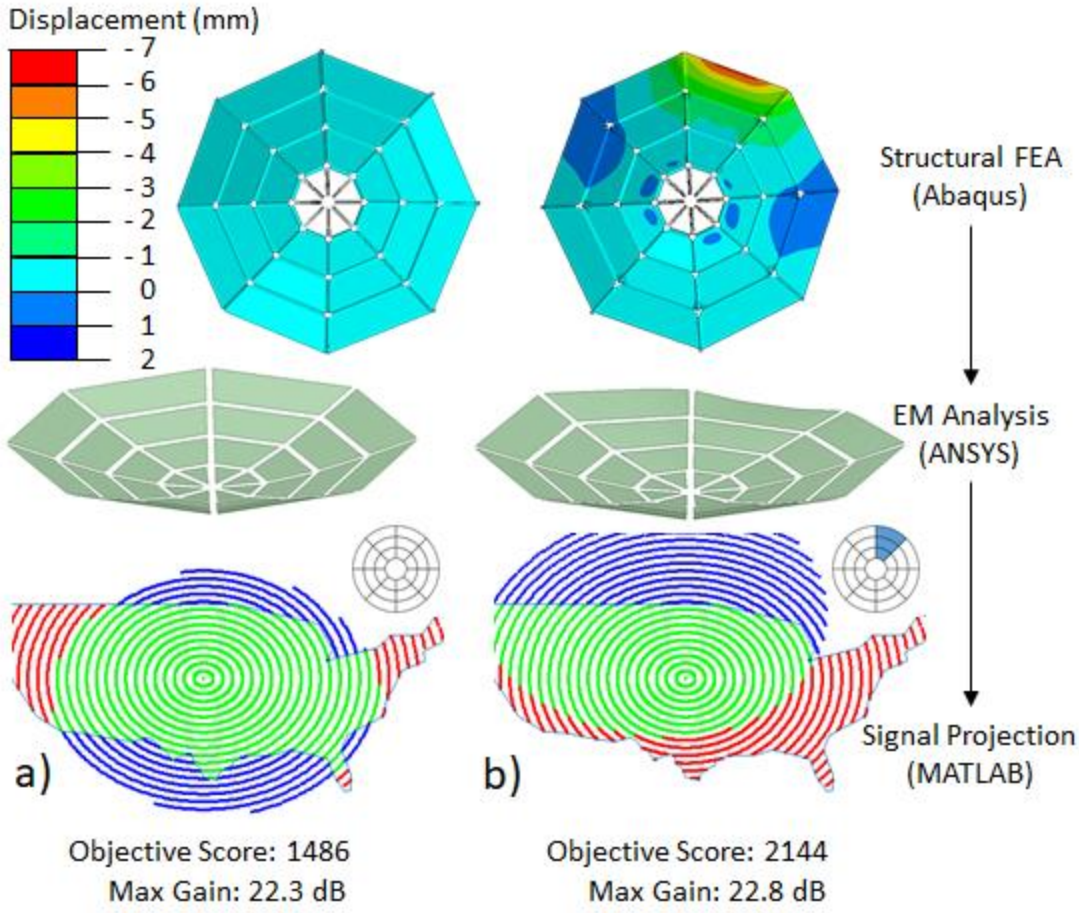

Figure 27: Difference between a) an undeformed ARORA and b) an ARORA with one slice undergoing max actuation

Figure 27 shows that the deformation of one slice of the antenna using wires each contracting by only 2.5% of their length has a major impact on the radiation pattern of ARORA. It should then follow that if the deformation of one specific part of the antenna can lead to massive changes in the projection of the signal onto a shape then finely tuning that deformation in strategic regions may lead to an actuation layout that could cause a radiation pattern to closely match a goal shape. In order to further prove this idea, two opposite slices of the antenna were actuated by their full amounts in order to transform the

discretized paraboloid into a shape that would possibly cause the antenna to transmit into a more elliptical pattern as seen in Figure 28. This highly deformed shape altered the radiation pattern even further than the antenna only undergoing actuation caused by one slice, and should serve as the most extreme case that might feasibly be used. It is possible to actuate all wires to 100% to make ARORA "blossom" and flatten out, but the electromagnetic results of such an antenna are so poor they do not represent an antenna that one would ever want to employ.

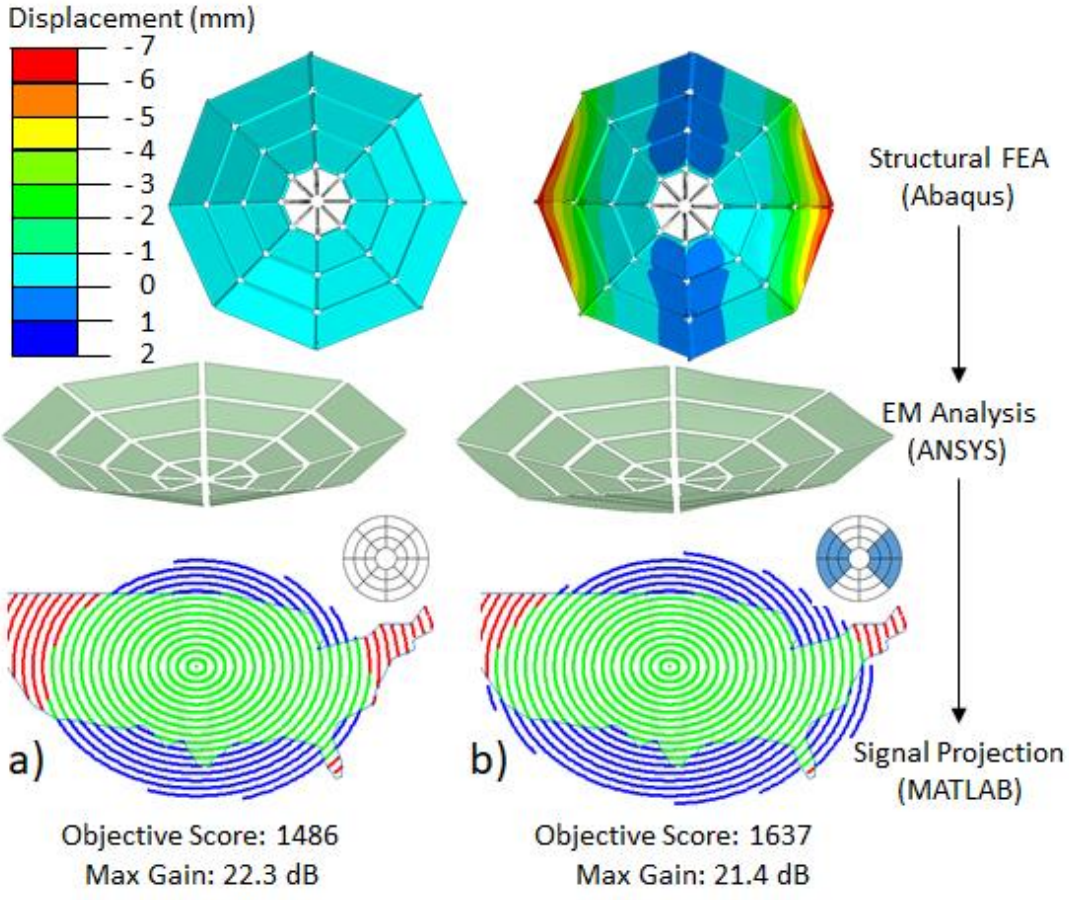

Figure 28: Comparison between a) an undeformed ARORA and b) an ARORA with two opposing sides undergoing maximum actuation

Experimental Validation

Structural validation for ARORA was done by constructing a simple 2x6 discretized antenna prototype for ease of fabrication, rather than a 4x8 antenna as seen in previous modeling. A 2x6 fold pattern was created using the tucked-folding methods presented in Chapter II, and then the pattern input into a laser cutter to trace out the three composite layers (2 paperboard, one polystyrene). The 3 layers were then bonded together using an epoxy and the flat configuration of the 2x6 ARORA was placed in an oven in order for the polystyrene to contract causing the folded and undeformed ARORA configuration to be created. 3D printed wire holders were then attached to the undersides of two adjacent faces of the antenna and a commercially available 0.3 mm diameter SmartFlex03 NiTi wire was threaded through the holders and crimped on its ends while trying to keep the wire as taut as possible. A speckle pattern was then applied to the two antenna faces so that 3D digital image correlation (DIC) could be used to determine the deformation of the antenna faces by comparing the location of pixels in the image throughout the actuation process. The antenna face opposite of the faces undergoing deformation was then clamped in place to serve as a boundary condition and the experiment was ready to be conducted.

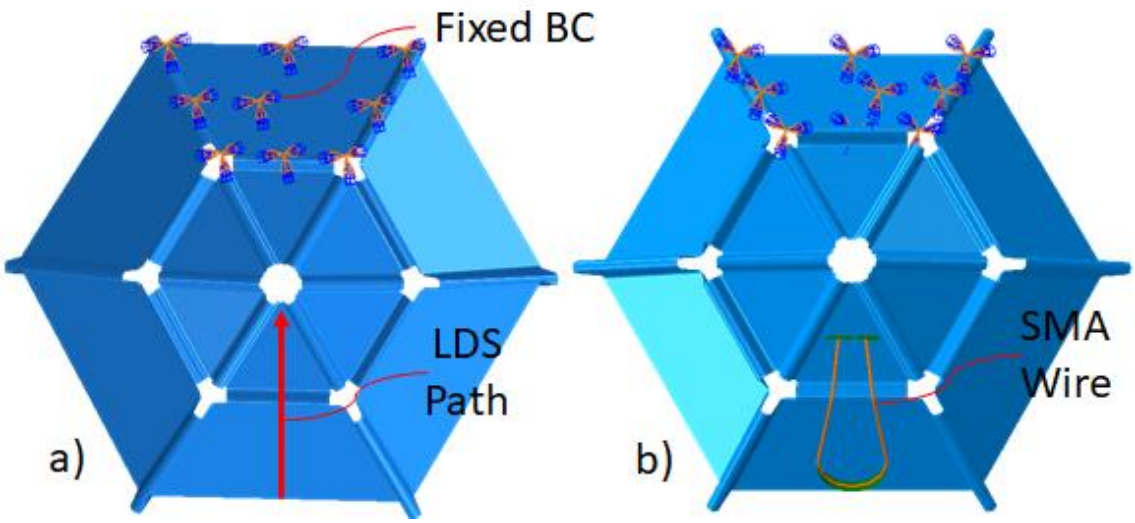

Figure 29a) Front view of 2x6 ARORA model to be validated b) Back view of ARORA model

Experimental results presented in this chapter utilized an LDS technique rather than DIC because it was difficult to capture out of plane deformations with the 3D DIC equipment available. The specifications of the LDS system are outlined in Chapter II. Only the positions of the centerline of the faces are presented here as a validation for the model as the heat from the SMA wire on the prototype began to melt the ABS plastic structure and more prototypes would have been needed to test the behavior of locations other than the facet centers.

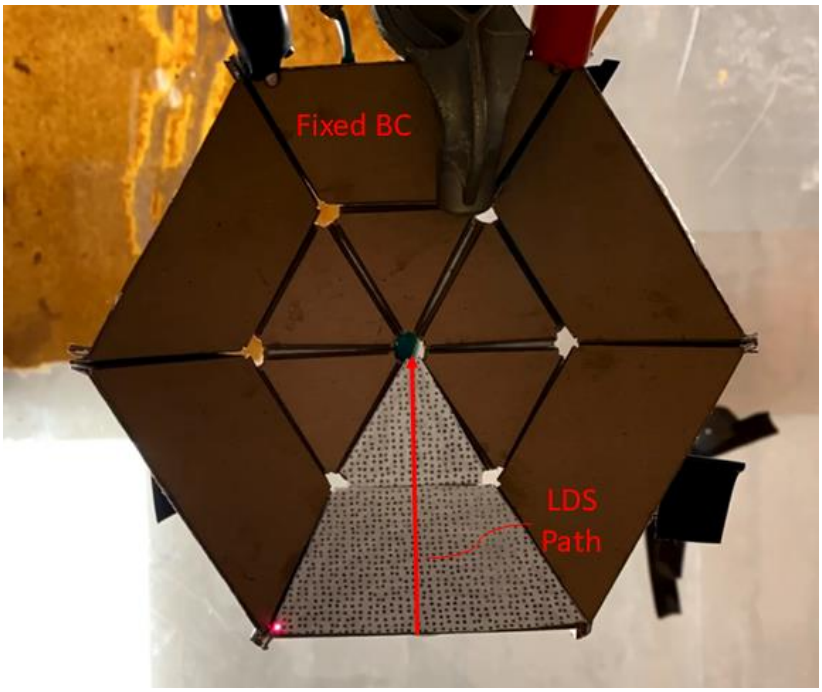

Figure 30: Front view of experimental setup

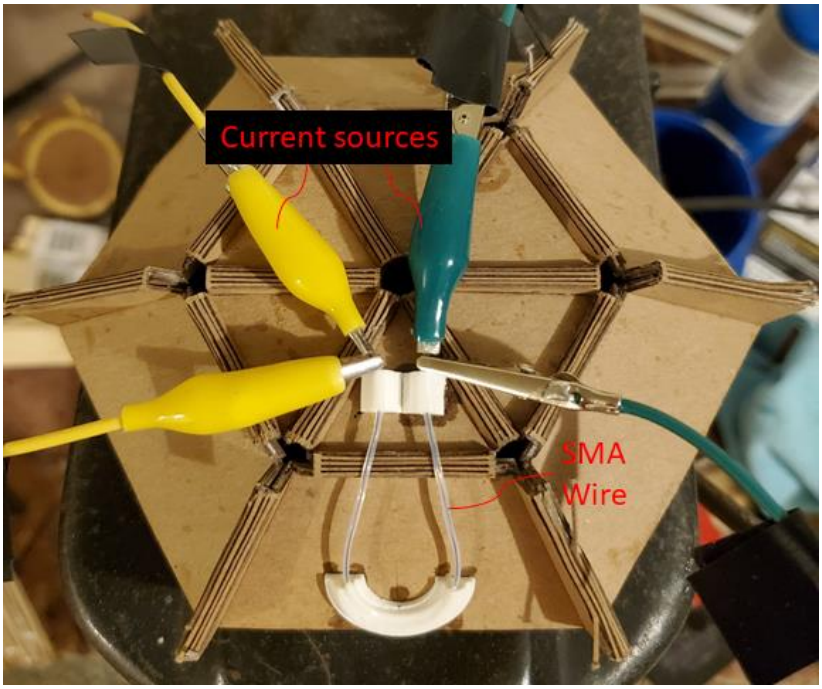

Figure 31: Back view of experimental setup

The SMA wire was heated via Joule heating by creating a 0.1 A current within the wire and varying the voltage within the wire from 0 V to 3.1 V causing the wire to raise in temperature. 3.1 V was used as the limit voltage because the wire would visibly contract at this setting and the insulation around the wire was hot to the touch. It is possible that more power could have been supplied to the SMA to heat it even further, but this was not done in order to preserve the ABS plastic wire holders which have a relatively low melting point [54]. Furthermore, as the commercial used NiTi has a starting transformation temperature of 30˚C, it was assumed that the wire could be considered to be undergoing a transformation from martensite to austenite since it was hot to the touch through an insulative coating. However, since no finishing transformation temperature was listed for this wire, there is no way to determine if the wire ever reached a temperature that achieved the advertised 5% actuation strain. For these reasons, the experimental results of the antenna deformation were compared against a 2x6 model undergoing various amounts of actuation from 0% - 5% to determine a feasible amount of actuation strain to be used in a design study to match a deformed antenna to a desired signal area.

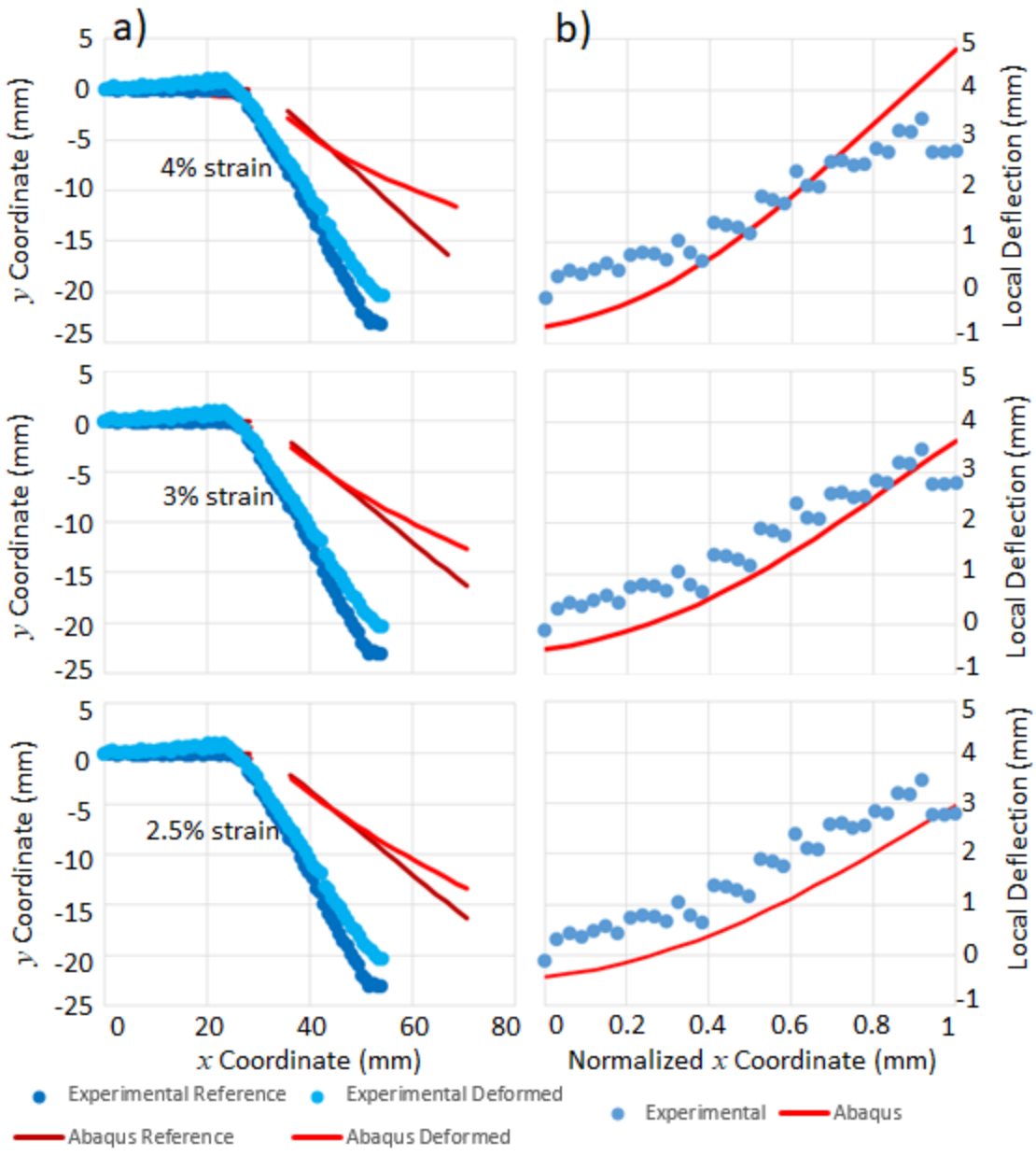

Figure 32a) depicts the differences between the shape of the experimental prototype and Abaqus model before and after deformation b) presents the deflection of the outer facet in normalized *x* coordinates

Overall, the deformations of the experiment correspond the greatest with the ARORA model undergoing a 2.5% actuation strain implying that the physical wire likely

achieved a similar amount of strain. The most obvious difference between the deformed states of the model and the behavior of the prototype is the curvature of the outer facet which appears to be undergoing a sort of warping due to bending. This warping might be attributed to the lack of the epoxy bonding within the Abaqus ARORA model that could provide some structural support and resistance to bending, or it may be because of the significant difference in the initial undeformed states of the prototype and model. The prototype's folds exhibited a more acute angle than the model, and differences in the fold angles would cause a change in the amount of moment applied to the tucked-fold region on the underside of the antenna. These differences in moment could account for the forces on the facet causing a warping in the model rather than the type of rigid body rotation seen in the experiment.

Different reference (undeformed) fold angles could have been modeled and the analysis could have been conducted again, but that was believed to be unnecessary for the validation process. The origami design codes used to generate origami models in this research generate fold patterns and folded geometries that most closely match the desired goal geometry (i.e. the output of the MATLAB code from [39]). The more acute fold angles seen in the experiment represent an error associated with the transition of polystyrene used to fold the origami structure from glassy to rubbery, which tends to generate more deformation than the fold pattern design tool predicts. The discrepancies and inconsistencies for the polystyrene material and composite layup cause the antenna to exhibit the "over-folding" behavior visualized in Figure 32. A new model could have been generated based on the prototype created to more closely match the fold angles seen in

reality, but that would have been counterproductive as the entire purpose of this experiment was to validate the actuation deformations seen measured in the more complex and difficult to produce 4x8 ARORA model, and not the accuracy of the polystyrene driven self-folding deformations. Regardless of the difference in reference configurations between the model and the experiment, both deformed configurations exhibit a similar warping behavior. In the end, it was decided that the ARORA prototype validated the structural behavior particularly at an actuation strain of 2.5% and optimization of actuation techniques to match a desired shape could be carried out as planned.

Electromagnetic validation on a deformed antenna was unable to be performed in this work and is left for future work if the development of this reflector were to go further. However, experiments to find the radiation pattern of the simple 2x6 discretized antenna were done by Jape et. al by coating the facets of the antenna with a reflective copper tape [68]. The aforementioned work showed the 2x6 antenna's signal pattern closely matched an EM model that used the same conditions and settings as seen in Chapter II. It was assumed no further experimentation would be required because the methods for creating the EM models in this work were kept consistent with previously validated models.

CHAPTER IV DESIGN STUDY

Three total design studies were performed in order to demonstrate the power of the modeling and optimization tools used. First, the effects of using increasingly more actuators with the EGO algorithm towards matching a signal to the CONUS shape was studied. Then, lessons learned from the CONUS analyses were applied to shaping a signal to the shape of China. Finally, EGO was applied using all previously explored designs towards broadcasting to the area of the state of Texas. The design process is outlined in the 5 step process below:

1. Create a design space comprised of actuation amounts for each SMA wire using the 10 x k standard number of initial designs explained by EGO PAPER et. al [63]
    1a. Repeat steps 2-4 until all initial designs have an objective score associated with them. This “initializes” the design space.
2. Perform structural FEA in Abaqus on the origami antenna using the actuation amounts for the current set of design variables.
3. Import the deformed shape from Abaqus into ANSYS-HFSS in order to export the radiation pattern of the irregular antenna shape.
4. Project the radiation pattern of the deformed antenna onto the goal broadcast area and calculate the antenna’s objective score.
5. After repeating 2-3 for the initial design space, begin adding design points using the EGO algorithm, repeating steps 4-6, until convergence to an optimal actuation amount for each actuator has been achieved.

All steps of the design process are looped through a MATLAB script that autonomously executes the analysis software and computes the new designs to be created via the EGO algorithm.

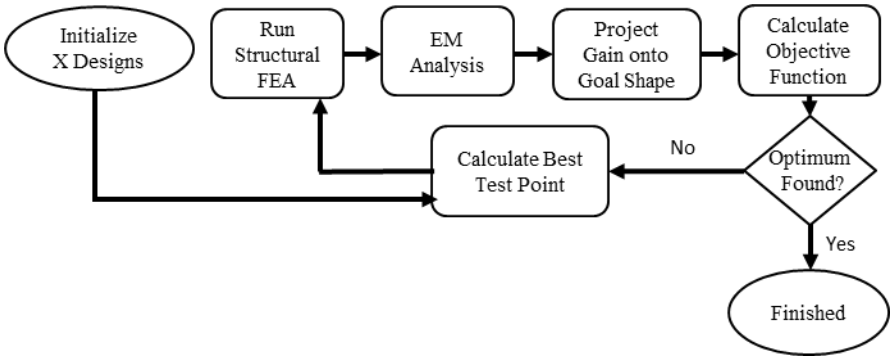

Figure 33: Flow chart of the optimization process

United States Study and Results

The first study carried out was the simplest study done. Only the eight inner most faces were allowed to undergo actuation as they were determined to have the largest effect on the overall displacements of the antenna as discussed in Chapter III. 80 sets of eight design variables each ranging from 0% to 100% were initialized while the remaining 16 variables were left at 0%.

$$[x,x,x,x,x,x,x,x,0,0,0,0,0,0,0,0,0,0,0,0,0,0,0,0]; \ 0 \leq x \leq 1$$

No points within the initial exploration of designs for only 8 DVs outperformed a basic undeformed ARORA. However, the EGO algorithm found a design that exceeded all initially explored points and the performance of the undeformed ARORA after the addition of only one point. The evolution of only the designs that improved the objective

function in chronological order can be seen in Figure 34b). The EGO algorithm appears to find progressively better designs relatively early in the optimization process but as the objective score improves it takes more additional points between improvements implying that is getting more difficult to find better designs. 420 points were explored through EGO to bring the total number of eight DV designs explored to 500, and all CONUS designs for ARORA will also total to 500 for each respective amount of actuators used.

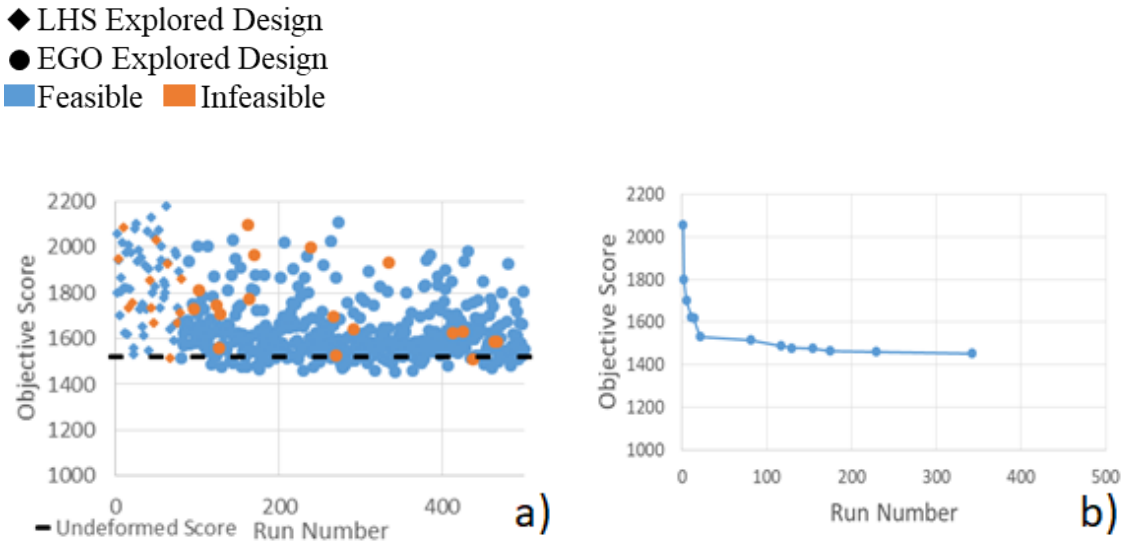

Figure 34a) Objective score of all tested 8 DV designs for CONUS b) History of designs that improved upon the previous best performance.

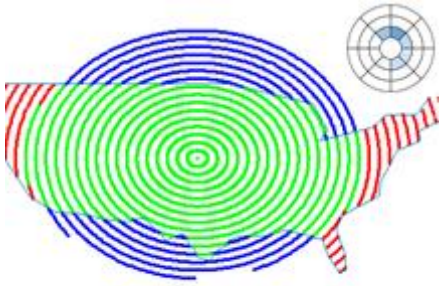

Figure 35: Projection of the best 8 DV ARORA onto CONUS

It can already be seen that the use of only eight DVs can improve the matching of ARORA past that of an antenna utilizing no SMA wires, but the improvements are marginal with only a 4% reduction in objective score found after a total of 500 designs were explored totaling over 300 hours of computer hours. In order to find an actuation technique that could significantly outperform an antenna with no actuators, a more complex 16 DV design space was introduced. This design space made use of the eight inner most SMA wires and the eight outermost SMA wires in hopes that the extra morphing capability would allow for more variability in the reflector shapes produced. The best design found with 16 DVs exhibited a 16% reduction in objective score beyond that of a simple undeformed ARORA, and a much more significant number of total designs explored by both EGO and the initial LHS exploration exceeded the undeformed score. A possible reason for this is that ARORA may start to resemble a true parabolic reflector after actuation because each SMA actuator is contracting causing the flat facets of ARORA to warp outward becoming curved and improving the overall performance of the antenna. This idea is explored further when all possible actuators are used.

$$[x,x,x,x,x,x,x,x,0,0,0,0,0,0,0,0,x,x,x,x,x,x,x,x]; \; 0 \leq x \leq 1$$

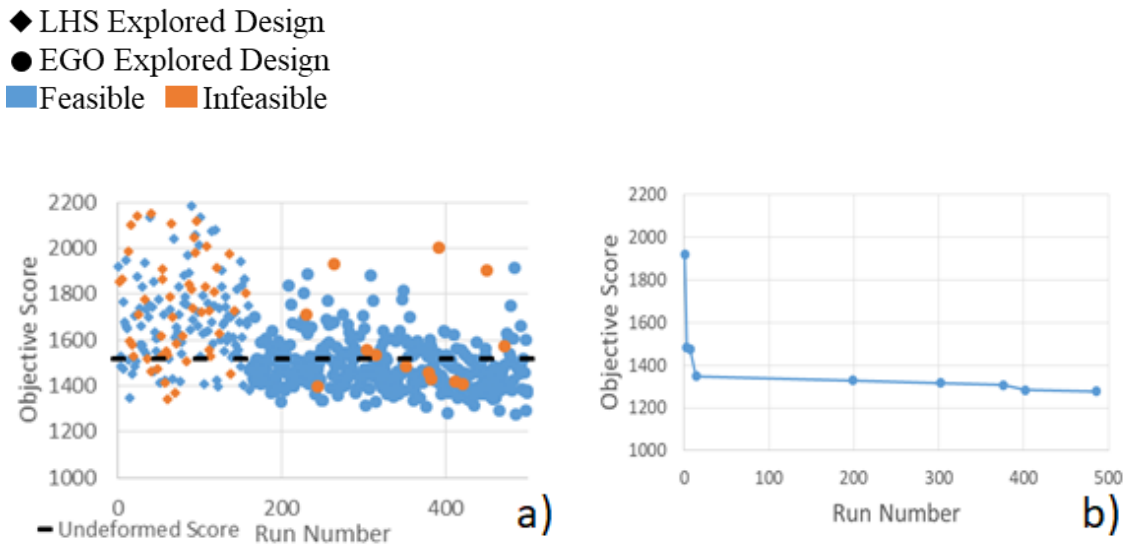

Figure 36a) Objective score of all tested 16 DV designs for CONUS b) History of designs that improved upon the previous best performance.

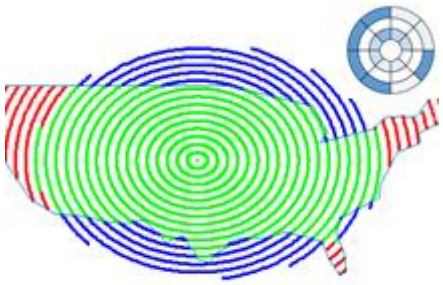

Figure 37: Projection of the best 16 DV ARORA onto CONUS

The already complex design space of eight and 16 DVs is made even more complex by the addition of the final eight possible SMA wires into the optimization process. An LHS of 240 designs was populated just as it was with the previous two optimizations in accordance to step three of the optimization framework. However, in the case of this 24 DV ARORA optimization, the EGO algorithm used all previous 1000 designs from the 500 eight DV and 16 DV optimizations, respectively, along with the 240

LHS points to initiate its surrogate model. Because of this, the EGO process of calculating the best possible test points begins to take the bulk of the computational time which was previously the process of solving for the deformations of the antenna through FEA in Abaqus. Times between the addition between points start to exceed 50 minutes with 24 DVs when considering all previously 1000 designs rather than averaging about 35 minutes for the eight DV optimization that began with only the 80 initially explored designs. The evolution history of designs in this case is more difficult to visualize, but Figure 38 attempts to show that the previous designs for simpler ARORA cases influence the EGO algorithm for 24 DVs in addition to its initial LHS designs.

$$[x,x,x,x,x,x,x,x,x,x,x,x,x,x,x,x,x,x,x,x,x,x,x,x]; 0 \leq x \leq 1$$

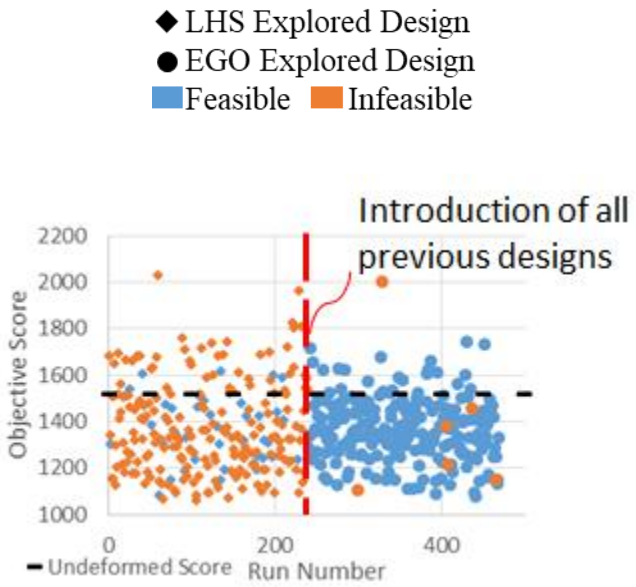

Figure 38: Objective score of all tested 24 DV designs for CONUS

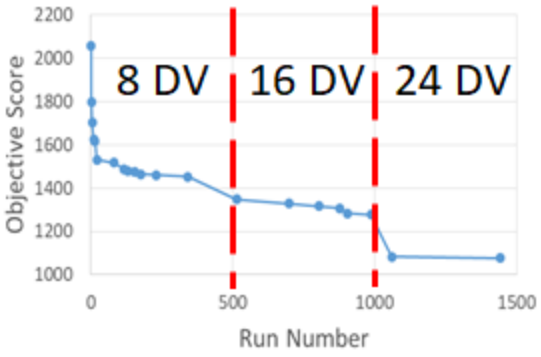

Figure 39: History of designs that improved upon the previous best performance

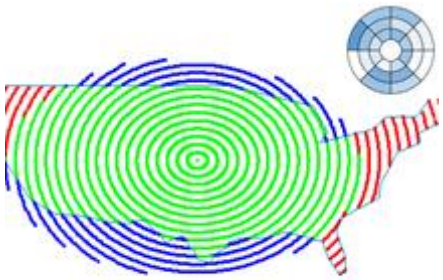

Figure 40: Projection of the best 24 DV ARORA onto CONUS

It is immediately apparent from the evolution history of 24 DVs that the use of many actuators brings a majority of designs under the objective score of an antenna with no actuators in use. Additionally, and fascinatingly, the EGO algorithm only explored six infeasible designs after considering 1240 previous designs where 200 of the 240 LHS points for the most complex case were infeasible. This shows the ability for EGO to explore the feasible space well and avoid penalties for its objective function. The overall best design to match CONUS found in this design study was utilizing all 24 DVs that exhibited a 29% total improvement over the undeformed ARORA. It would be possible to run the optimization for a longer time to possibly find an even better design than the one

found, but that is left to be done at another time as the utility of the EGO algorithm can be further exemplified when the same algorithm, antenna, and process are applied to match other shapes better than a basic undeformed antenna could.

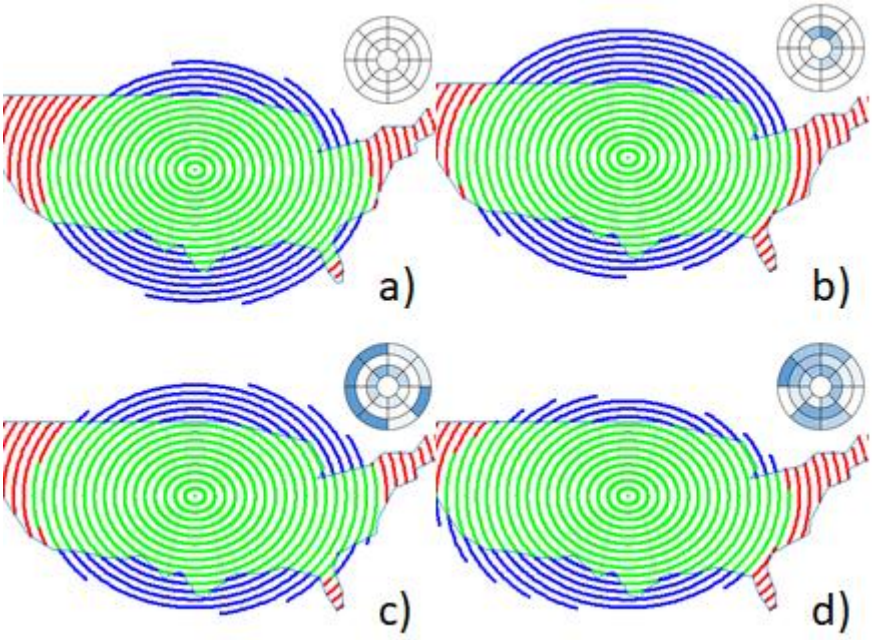

Figure 41a) Undeformed ARORA projected onto CONUS b) Best 8 DV ARORA projection c) Best 16 DV ARORA projection d) Best 24 DV ARORA

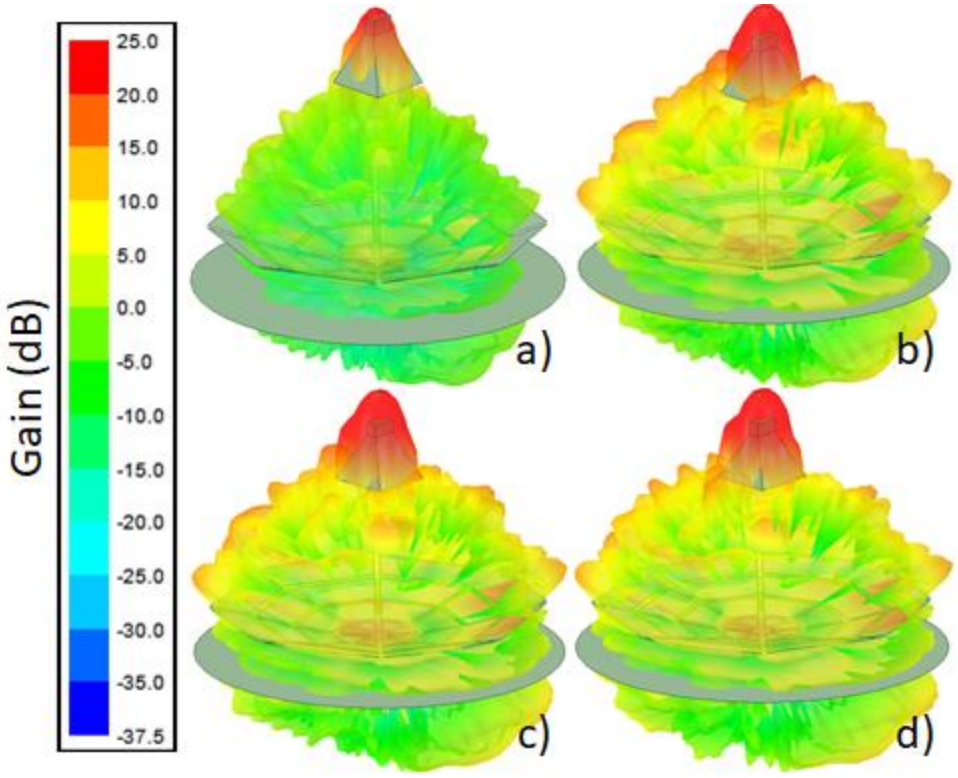

Figure 42a) 3D polar gain plot of an undeformed ARORA b) Gain plot of the best 8 DV ARORA c) Gain plot of the best 16 DV ARORA d) Gain plot of the best 24 DV ARORA

Antenna	Objective Score	Maximum Gain
Ideal Parabolic Reflector	1558	23.7 dB
Undeformed ARORA	1519	22.3 dB
8 Wire ARORA	1454	22.8 dB
16 Wire ARORA	1278	22.8 dB
24 Wire ARORA	1077	22.9 dB

Table 5: Performance characteristics for various antennas projected onto the CONUS shape

China Study and Results

China was chosen as another goal shape to match a signal to because it is of a similar size and relative complexity as the shape of CONUS. Two studies overall were conducted towards matching a broadcast area of China. The first study was solely EGO driven without a robust initial design space that showcases the ability for the EGO algorithm to find designs by itself. The other study used all previous designs (including those found by the EGO driven exploration), but the signal patterns found while matching the CONUS shape were instead projected onto the shape of China. Every actuation technique explored can be applied to any other goal shape, all that is needed is to remap the values of the objective function using the appropriate broadcast areas so that the same input DVs could have different outputs based on a new projection.

Purely EGO driven exploration for about 400 points of the design space to match China was conducted using all 24 possible actuators with no real surrogate model to begin searching for the best designs to test. The study was stopped prior to reaching 500 points because EGO was unable to avoid infeasible designs nearly as well as it can with a proper starting surrogate model with only 44 designs of the 376 sets of inputs being feasible. However, the feasible sets of inputs that the algorithm managed to find designs that were comparable to the 24 DV designs found for CONUS when projected onto China instead. CONUS designs appear to do well for China as well because of the two countries' relatively similar shapes. These EGO explored designs will be used to initialize the surrogate for the next China design study along with all previous CONUS designs for eight, 16, and 24 DVs projected onto China. It should be noted that the overall objective

score is larger for ARORA when projecting onto China due to the country being larger, and this does not imply that the EGO algorithm is any worse at matching one country than it is another.

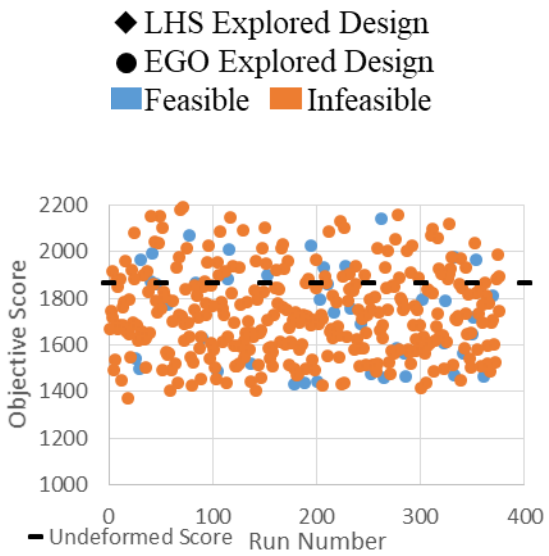

Figure 43: Optimization history of the purely EGO driven exploration of the design space to match China

Beginning with an initial design space composed of 1816 design points for China, the EGO algorithm then added 434 more design points to begin to find a set of inputs that could allow ARORA to more closely match its desired broadcast area. Several more designs were found that exceeded any feasible point used to form the initial surrogate of the algorithm, and nearly all designs outperformed the performance of an undeformed discretized antenna just as was the case with the 24 DV study done for CONUS. However, it can be seen that the amount of additional designs needed to be tested prior to finding a combination of actuation amounts that improves the objective increases again compared to the more simple studies that did not need to search for a better test point in as large of

a design space. This study does exemplify the ability for EGO to take any previously applicable design into account when attempting to optimize to a different objective function thus further showcasing the utility of the algorithm. The aforementioned utility is then expanded upon even further when all actuation techniques tested, be it for CONUS or China, are then used to begin an optimization study towards finding a design that could match the state of Texas.

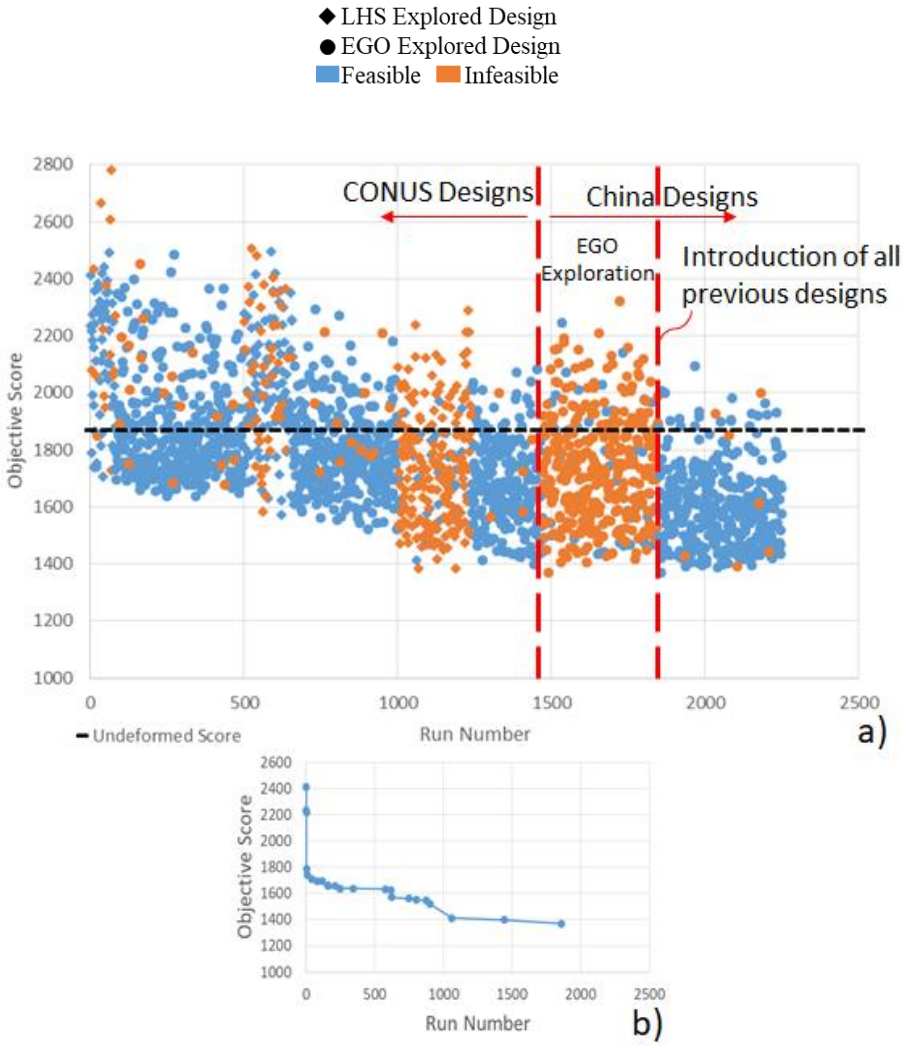

Figure 44a) Objective score of all tested designs projected onto China b) History of designs that improved upon the previous best performance.

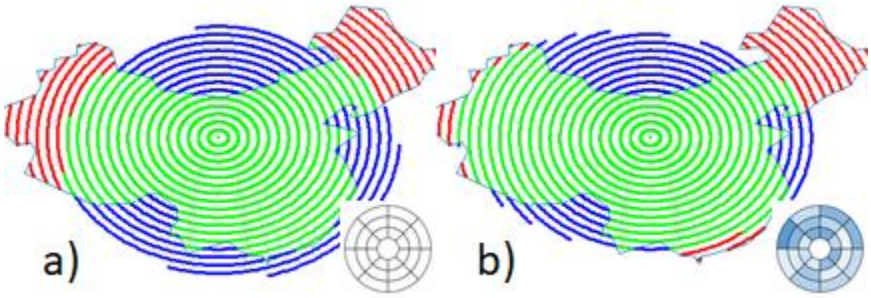

Figure 45: Comparison between the projection of a) the undeformed ARORA and b) the best performing ARORA projected onto China

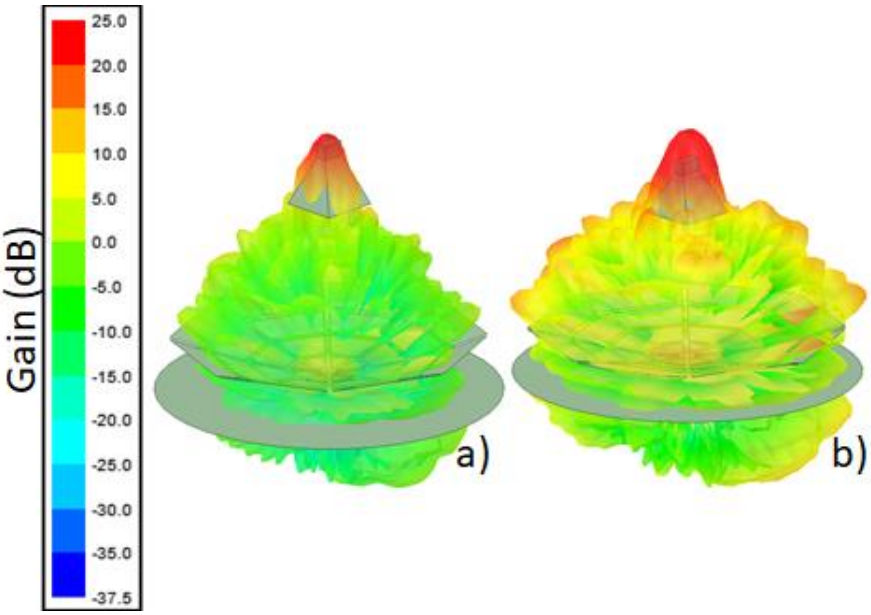

Figure 46a) 3D polar gain plot of the undeformed ARORA b) Gain plot of the best performing ARORA for China

Antenna	Objective Score	Maximum Gain
Ideal Parabolic Reflector	1700	23.7 dB
Undeformed ARORA	1869	22.3 dB
China Optimum ARORA	1368	23.0 dB

Table 6: Performance characteristics for various antenna projected onto the shape of China

Texas Study and Results

All previously tested 2250 designs for all levels of complexity in design variables and studies for both CONUS and China were used to initialize a surrogate model to begin the EGO process towards finding a strategy that could project onto the state of Texas. After the signal patterns for the previous designs were projected onto Texas from an altitude of 6500 km (altitude had to be lowered as the beamwidth of the antenna was designed for matching CONUS at an altitude of 25000 km), the best antenna that matched the Texas shape from the previous tests was actually from the EGO driven exploration of China. Test points were then calculated via the EGO algorithm which began taking a significant part of the run time as an optimal design point had to be found from over 2000 points in a 24 dimensional space. The time between completions of the analysis of two designs went from averaging about 35 minutes for the simpler eight DV design spaces with less than 500 points to search from to about 65 minutes for the case of this Texas study.

The complexity of the design space used for Texas led to some difficulties for the EGO algorithm discovering a better set of actuation amounts than the ARORA designs that had already been completed. Only one feasible design out of the 750 possible designs tested by EGO for the state of Texas was found that exceeded any previous design, and the improvement was a marginal three point reduction in the objective score beyond the previous best. However, if the constraints that determined the feasibility of a design were relaxed, then at least one design would have been found that showed an improvement of

about 3% beyond any previous point found. The overall best infeasible design found by EGO had a stress of 663 MPa, just exceeding the constraint of 650 MPa meant to represent the yield stress of the NiTi wires being used. If a material with a higher yield stress were to be implemented into this study, or the stress constraints were removed entirely and a material that could withstand the strains shown were selected post-hoc there may have been even better performing designs found throughout the studies. As it stands, the three designs outlined in this chapter exemplify the capability of the EGO algorithm and the effect just a small amount of actuation can have on the signal pattern of an antenna towards the shape matching of a desired area.

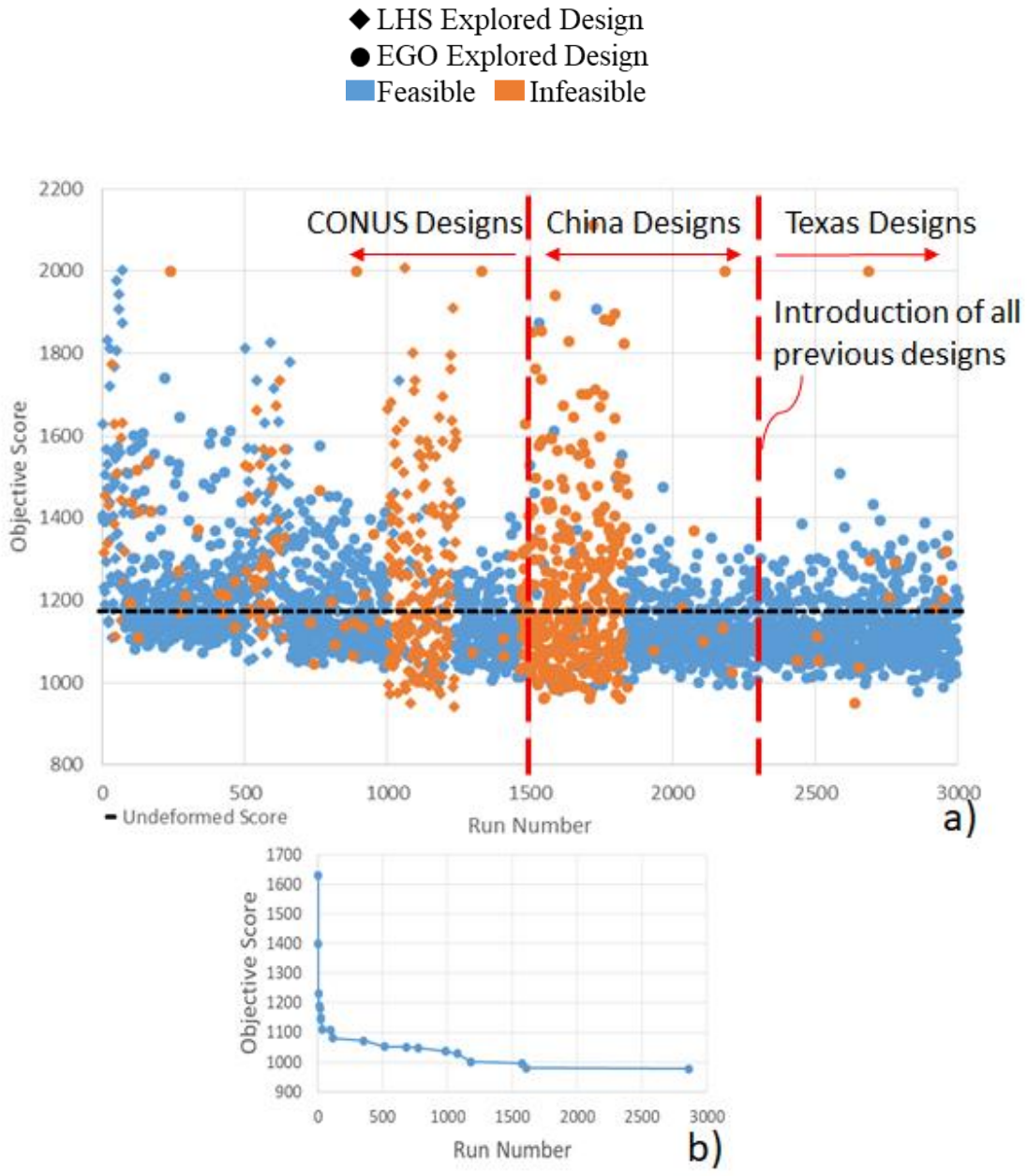

Figure 47 a) Objective score of all tested designs projected onto Texas b) History of designs that improved upon the previous best performance.

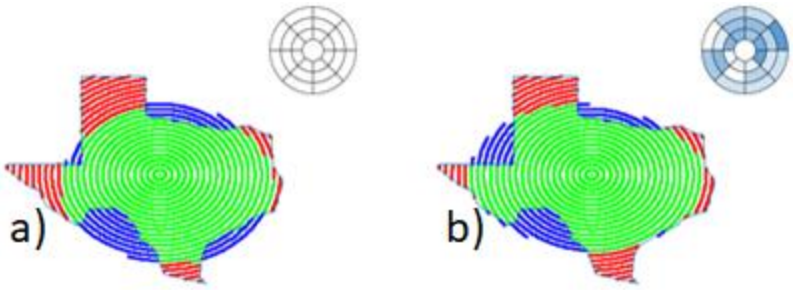

Figure 48: Comparison between the projection of the a) undeformed ARORA and b) best performing ARORA projected onto Texas

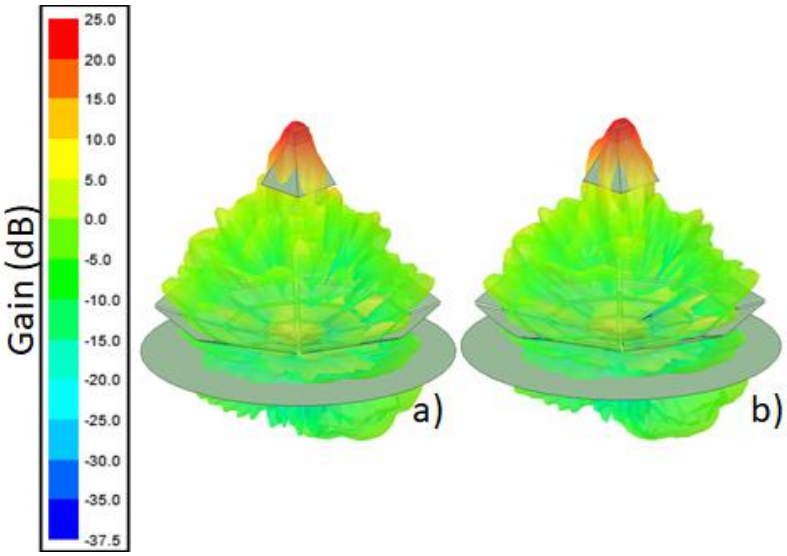

Figure 49a) 3D polar gain plot of the undeformed ARORA b) Gain plot of the best Texas ARORA

Antenna	Objective Score	Maximum Gain
Ideal Parabolic Reflector	1105	23.7 dB
Undeformed ARORA	1174	22.3 dB
Texas Optimum	977	22.3 dB

Table 7: Performance characteristics for various antenna projected onto the shape of Texas

CHAPTER V

CONCLUSIONS AND FUTURE WORK

ARORA models utilizing actuating SMA wires on just the underside of the discretized parabolic reflector showcase the ability for the same antenna structure to project its signal onto different desired areas by varying the level of actuation of specific wires. The general structural behavior of the model was able to be validated experimentally for a case with a single actuator spanning one fold so it should follow that the addition of more wires about other folds would behave in a way predicted by the structural FEA. No electromagnetic validation was done for any of the deformed antennas done in this work, but the same modeling techniques were done for the undeformed ARORA that had been previously validated by Jape et. al [65]. The simplifications used in structural modeling reduced computational time and did not compromise the integrity of the found solutions. The aforementioned simplifications allowed the EGO algorithm to find actuations strategies that far exceeded a discretized antenna's capability to match a signal pattern with just 3000 designs tested over five total design studies.

EGO served as a great optimization tool for this research. The high dimensionality of the design space would have required thousands of sets of DVs to be used in order to use a robust heuristic optimization algorithm. However, with EGO good designs were able to be found in fewer than 200 iterations in some cases due to the ability to strategically search for points within a design space with an expected improvement to the objective function while avoiding designs that would violate constraints. About 2500 computational

hours were used overall during the 3000 unique tests so it was important to minimize the amount of total analyses used throughout the optimization process in order to find a design in a reasonable amount of time. Any of the design studies could be started exactly where they were stopped and continue towards finding even better actuation strategy, but due to time constraints the DVs found for each study are taken to be optimal for the purpose of this research. Additionally, the 3000 tested designs would provide a good starting point towards optimizing another goal signal shape just as was seen when the previous designs for CONUS were employed to find designs for China and then the state of Texas as well.

A single ARORA could have the capability to alter its signal pattern on demand to more closely match an area of operations by inputting a calculated actuation strategy. Possible implementation would involve creating a working library of actuation techniques for respective countries or areas that an antenna may need to broadcast to then controlling the SMA actuators to transition between them. This idea could be useful on something like an orbiting satellite that could be above several different areas during its orbit in order to change shape accordingly. The projection could even be altered to project from a point that is not directly above the centroid of the desired shape, so a library of DVs could be created that change the antenna dynamically to track the shape of the area as the satellite passes. The ability to send signal to only the areas it is desired has implications for the security sector as well. An antenna could be used to only send a signal to an area where there is an allied military operation so that an enemy force cannot intercept it. ARORA could be stored in its flat configuration for the military transport, then deployed and controlled in the field by an engineer to send signals to those on the front lines.

The capabilities of ARORA are impressive, but there are possible improvements that should be considered if the antenna were to be improved upon even further or brought closer to implementation in a real environment. Ideas for future improvements are presented in the future work section of this thesis and should possibly be considered by anyone who wishes to continue to improve upon the ARORA idea.

Future Work

- Perform validation for the signal pattern of deformed ARORA prototypes.
- More rigorously model the transformation and characteristics of SMA for actuation of the antenna.
- Find a way to script the addition of fold regions into ANSYS models for deformed antennas.
- Solve an uncoupled version of the problem posed in this research i.e. find the best shape that an antenna should have to match a broadcast area and then determine the actuation techniques in order to achieve that specific deformed shape.
- Start from a different reference geometry e.g. a patch or microstrip antenna.
- Apply other optimization techniques to the design process to compare the total runtimes required for EGO versus other heuristic algorithms.

REFERENCES

[1] Visser, Hubregt, J. Antenna Theory and Applications. Chichester, UK: John Wiley & Sons, Ltd, 2012. https://doi.org/10.1002/9781119944751.fmatter.

[2] Cherrette, A.R., S.-W. Lee, and R.J. Acosta. "A Method for Producing a Shaped Contour Radiation Pattern Using a Single Shaped Reflector and a Single Feed." *IEEE Transactions on Antennas and Propagation* 37, no. 6 (June 1989): 698–706. https://doi.org/10.1109/8.29356.

[3] Washington, Gregory, and Larry Silverberg. "Modal Control of a Corner Reflector to Maximize Far-Field Power." *Microwave and Optical Technology Letters* 8, no. 5 (April 5, 1995): 260–64. https://doi.org/10.1002/mop.4650080513.

[4] Washington, Gregory. "Smart aperture antennas." *Smart Mater. Struct.* 5, no. 6 (August 1996): 801-805. https://doi.org/10.1088/0964-1726/5/6/010.

[5] Gupta, Vijay Kumar, P. Seshu, K. Kurien Issac, and R.K. Shevgaonkar. "Beam Steering and Shaping of Smart Cylindrical Antenna." *AIAA Journal* 43, no. 1 (January 2005): 165–73. https://doi.org/10.2514/1.8689.

[6] Hwan-Sik Yoon, G. Washington, and W. H. Theunissen. "Analysis and Design of Doubly Curved Piezoelectric Strip-Actuated Aperture Antennas." *IEEE Transactions on Antennas and Propagation* 48, no. 5 (May 2000): 755–63. https://doi.org/10.1109/8.855494.

[7] Shun Yao, S. V. Georgakopoulos, B. Cook, and M. Tentzeris. "A Novel Reconfigurable Origami Accordion Antenna." In *2014 IEEE MTT-S International Microwave Symposium (IMS2014)*, 1–4, 2014. https://doi.org/10.1109/MWSYM.2014.6848571.

[8] Sarrazin, Julien, Yann Mahe, Stéphane Avrillon, and Serge Toutain. "Pattern Reconfigurable Cubic Antenna." *IEEE Transactions on Antennas and Propagation* 57, no. 2 (February 2009): 310–17. https://doi.org/10.1109/TAP.2008.2011221.

[9] Pozar, D. M., S. D. Targonski, and H. D. Syrigos. "Design of Millimeter Wave Microstrip Reflectarrays." *IEEE Transactions on Antennas and Propagation* 45, no. 2 (February 1997): 287–96. https://doi.org/10.1109/8.560348.

[10] Nayeri, Payam, Fan Yang, and Atef Z. Elsherbeni. "Bandwidth Improvement of Reflectarray Antennas Using Closely Spaced Elements." *Progress In Electromagnetics Research C* 18 (2011): 19–29. https://doi.org/10.2528/PIERC10091505.

[11] Cooley, Michael E, Newbury Park, Thomas J Chwalek, and Parthasarath Ramanujam. "Method For Improving Pattern Bandwidth of Shaped Beam Reflectarrays." n.d., 7.

[12] Rahmat-Samii, Y., and V. Galindo-Israel. "Shaped Reflector Antenna Analysis Using the Jacobi-Bessel Series." *IEEE Transactions on Antennas and Propagation* 28, no. 4 (July 1980): 425–35. https://doi.org/10.1109/TAP.1980.1142364.

[13] Washington, Gregory, and Larry Silverberg. "Modal Control of a Corner Reflector to Maximize Far-Field Power." *Microwave and Optical Technology Letters* 8, no. 5 (April 5, 1995): 260–64. https://doi.org/10.1002/mop.4650080513.

[14] Washington, Gregory. "Smart Aperture Antennas." *Smart Materials and Structures* 5, (August 1996): 801-805.

[15] Jacobs, S, C Coconnier, D DiMaio, F Scarpa, M Toso, and J Martinez. "Deployable Auxetic Shape Memory Alloy Cellular Antenna Demonstrator: Design, Manufacturing and Modal Testing." *Smart Materials and Structures* 21, no. 7 (July 1, 2012): 075013. https://doi.org/10.1088/0964-1726/21/7/075013.

[16] Lan, Xin, Jinsong Leng, and Shanyi Du. "Design of a Deployable Antenna Actuated by Shape Memory Alloy Hinge," n.d., 5.

[17] Lagoudas, Dimitris C., ed. *Shape Memory Alloys: Modeling and Engineering Applications*. New York, NY: Springer, 2008.

[18] Shu, Steven G, Dimitris C Lagoudas, Declan Hughes, and John T Wen. "Modeling of a flexible Beam Actuated by Shape Memory Alloy Wires," n.d., 13.

[19] Song, Gangbing, Brian Kelly, Brij N. Agrawal. "Active Position Control of a Shape Memory Alloy Wire Actuated Composite Beam." *Smart Materials and Structures* 9, (August 2000): 711-716.

[20] Jayender, J., R. V. Patel, S. Nikumb, and M. Ostojic. "Modeling and Control of Shape Memory Alloy Actuators." *IEEE Transactions on Control Systems Technology* 16, no. 2 (March 2008): 279–87. https://doi.org/10.1109/TCST.2007.903391.

[21] Chawla, A., B. Bhattacharya, and B. S. Munjal. "Optimal Actuation of SMA-Wire Network for Adaptive Shape Control of a Space Antenna System." In *2014 13th International Conference on Control Automation Robotics Vision (ICARCV)*, 306–11, 2014. https://doi.org/10.1109/ICARCV.2014.7064323.

[22] Weck, O. de, D. Miller, and J. Hansman. "Multifunctionality in Parabolic RF Antenna Design Based on SMA Actuated Radiation Pattern Shaping." In *7th AIAA/USAF/NASA/ISSMO Symposium on Multidisciplinary Analysis and Optimization*.

St. Louis,MO,U.S.A.: American Institute of Aeronautics and Astronautics, 1998. https://doi.org/10.2514/6.1998-4813.

[23] Mahdavi, Siavash Haroun, and Peter J Bentley. “Evolving Noise Tolerant Antenna Configurations Using Shape Memory Alloys,” n.d., 6.

[24] Tanaka, Hiroaki. “Surface Error Estimation and Correction of a Space Antenna Based on Antenna Gainanalyses.” *Acta Astronautica* 68, no. 7–8 (April 2011): 1062–69. https://doi.org/10.1016/j.actaastro.2010.09.025.

[25] Jalali Mazlouman, Shahrzad, Alireza Mahanfar, Carlo Menon, and Rodney G. Vaughan. “Reconfigurable Axial-Mode Helix Antennas Using Shape Memory Alloys.” *IEEE Transactions on Antennas and Propagation* 59, no. 4 (April 2011): 1070–77. https://doi.org/10.1109/TAP.2011.2109686.

[26] Hawkes, E., B. An, N. M. Benbernou, H. Tanaka, S. Kim, E. D. Demaine, D. Rus, and R. J. Wood. “Programmable Matter by Folding.” *Proceedings of the National Academy of Sciences* 107, no. 28 (July 13, 2010): 12441–45. https://doi.org/10.1073/pnas.0914069107.

[27] Peraza Hernandez, Edwin A., Darren J. Hartl, Ergun Akleman, and Katherine Frei. “Connectivity of Shape Memory Alloy-Based Self-Folding Structures.” In *22nd AIAA/ASME/AHS Adaptive Structures Conference*. National Harbor, Maryland: American Institute of Aeronautics and Astronautics, 2014. https://doi.org/10.2514/6.2014-1415.

[28] Nakanishi, Hiroki, Hiraku Sakamoto, Hiroshi Furuya, Masahiko Yamazaki, Yasuyuki Miyazaki, Akihito Watanabe, Kazuki Watanabe, Ayako Torisaka-Kayaba, and Mitsushige Oda. “Development of Nano-Satellite OrigamiSat-1 with Highly Functional Deployable Membrane,” n.d., 4.

[29] Sessions, Deanna M., Joshua T. Ruff, Francisco A. Espinal, Gregory H. Huff, Sameer S. Jape, E. A. Peraza-Hernandez, Dimitris C. Lagoudas, Darren J. Hartl, and Beatriz Borges. “Folding, Tessellation, and Deployment of an Origami-Inspired Active-Material-Enabled Self-Folding Reflector Antenna.” In *2018 IEEE International Symposium on Antennas and Propagation USNC/URSI National Radio Science Meeting*, 929–30, 2018. https://doi.org/10.1109/APUSNCURSINRSM.2018.8609355.

[30] Boatti, Elisa, Nikolaos Vasios, and Katia Bertoldi. “Origami Metamaterials for Tunable Thermal Expansion.” *Advanced Materials* 29, no. 26 (July 2017): 1700360. https://doi.org/10.1002/adma.201700360.

[31] Silverberg, J. L., A. A. Evans, L. McLeod, R. C. Hayward, T. Hull, C. D. Santangelo, and I. Cohen. “Using Origami Design Principles to Fold Reprogrammable Mechanical

Metamaterials." *Science* 345, no. 6197 (August 8, 2014): 647–50. https://doi.org/10.1126/science.1252876.

[32] Wang, Zuojia, Liqiao Jing, Kan Yao, Yihao Yang, Bin Zheng, Costas M. Soukoulis, Hongsheng Chen, and Yongmin Liu. "Origami-Based Reconfigurable Metamaterials for Tunable Chirality." *Advanced Materials* 29, no. 27 (July 2017): 1700412. https://doi.org/10.1002/adma.201700412.

[33] Nauroze, Syed Abdullah, Larissa S. Novelino, Manos M. Tentzeris, and Glaucio H. Paulino. "Continuous-Range Tunable Multilayer Frequency-Selective Surfaces Using Origami and Inkjet Printing." *Proceedings of the National Academy of Sciences* 115, no. 52 (December 26, 2018): 13210–15. https://doi.org/10.1073/pnas.1812486115.

[34] Fuchi, Kazuko, Philip R. Buskohl, Giorgio Bazzan, Michael F. Durstock, James J. Joo, Gregory W. Reich, and Richard A. Vaia. "Spatial Tuning of a RF Frequency Selective Surface through Origami." edited by Firooz A. Sadjadi and Abhijit Mahalanobis, 98440W. Baltimore, Maryland, United States, 2016. https://doi.org/10.1117/12.2224160.

[35] Shun Yao, S. V. Georgakopoulos, B. Cook, and M. Tentzeris. "A Novel Reconfigurable Origami Accordion Antenna." In *2014 IEEE MTT-S International Microwave Symposium (IMS2014)*, 1–4, 2014. https://doi.org/10.1109/MWSYM.2014.6848571.

[36] Sessions, Deanna, Kazuko Fuchi, Sumana Pallampati, David Grayson, Steven Seiler, Giorgio Bazzan, Gregory Reich, Philip Buskohl, and Gregory H. Huff. "INVESTIGATION OF FOLD-DEPENDENT BEHAVIOR IN AN ORIGAMI-INSPIRED FSS UNDER NORMAL INCIDENCE." *Progress In Electromagnetics Research M* 63 (2018): 131–39. https://doi.org/10.2528/PIERM17092504.

[37] Tachi, Tomohiro. "Geometric Considerations for the Design of Rigid Origami Structures," 2010, 12.

[38] Saito, Kazuya, Akira Tsukahara, and Yoji Okabe. "Designing of Self-Deploying Origami Structures Using Geometrically Misaligned Crease Patterns." *Proceedings of the Royal Society A: Mathematical, Physical and Engineering Science* 472, no. 2185 (January 2016): 20150235. https://doi.org/10.1098/rspa.2015.0235.

[39] Peraza Hernandez, Edwin A., Darren J. Hartl, and Dimitris C. Lagoudas. *Active Origami: Modeling, Design, and Applications*. Cham: Springer International Publishing, 2019. https://doi.org/10.1007/978-3-319-91866-2.

[40] Lo, Y.T., S.W. Lee, and Q.H. Lee. "Optimization of Directivity and Signal-to-Noise Ratio of an Arbitrary Antenna Array." *Proceedings of the IEEE* 54, no. 8 (August 1966): 1033–45. https://doi.org/10.1109/PROC.1966.4988.

[41] Schraml, K., R. Wilke, D. Heberling, and A. Narbudowicz. “Lightweight and Cost Efficient Spaceborn Patch Antenna.” In *2016 21st International Conference on Microwave, Radar and Wireless Communications (MIKON)*, 1–4, 2016. https://doi.org/10.1109/MIKON.2016.7491998.

[42] Teniente, Jorge, Ramon Gonzalo, and Carlos del Rio. “Satellite Horn Antennas Design.” In *2009 3rd European Conference on Antennas and Propagation*, 3081–84, 2009.

[43] Li, Tuanjie. “Deployment Analysis and Control of Deployable Space Antenna.” *Aerospace Science and Technology* 18, no. 1 (April 2012): 42–47. https://doi.org/10.1016/j.ast.2011.04.001.

[44] Genovesi, S., R. Mittra, A. Monorchio, and G. Manara. “Particle Swarm Optimization for the Design of Frequency Selective Surfaces.” *IEEE Antennas and Wireless Propagation Letters* 5 (2006): 277–79. https://doi.org/10.1109/LAWP.2006.875900.

[45] John, Matthias, and Max J. Ammann. “Antenna Optimization With a Computationally Efficient Multiobjective Evolutionary Algorithm.” *IEEE Transactions on Antennas and Propagation* 57, no. 1 (January 2009): 260–63. https://doi.org/10.1109/TAP.2008.2009775.

[46] Ares-Pena, F.J., J.A. Rodriguez-Gonzalez, E. Villanueva-Lopez, and S.R. Rengarajan. “Genetic Algorithms in the Design and Optimization of Antenna Array Patterns.” *IEEE Transactions on Antennas and Propagation* 47, no. 3 (March 1999): 506–10. https://doi.org/10.1109/8.768786.

[47] Kiziltas, G., D. Psychoudakis, J.L. Volakis, and N. Kikuchi. “Topology Design Optimization of Dielectric Substrates for Bandwidth Improvement of a Patch Antenna.” *IEEE Transactions on Antennas and Propagation* 51, no. 10 (October 2003): 2732–43. https://doi.org/10.1109/TAP.2003.817539.

[48] Al-Azza, Ali A., Ammar A. Al-Jodah, and Frances J. Harackiewicz. “Spider Monkey Optimization: A Novel Technique for Antenna Optimization.” *IEEE Antennas and Wireless Propagation Letters* 15 (2016): 1016–19. https://doi.org/10.1109/LAWP.2015.2490103.

[49] Cismasu, Marius, and Mats Gustafsson. “Antenna Bandwidth Optimization With Single Frequency Simulation.” *IEEE Transactions on Antennas and Propagation* 62, no. 3 (March 2014): 1304–11. https://doi.org/10.1109/TAP.2013.2295426.

[50] Robinson, J., and Y. Rahmat-Samii. “Particle Swarm Optimization in Electromagnetics.” *IEEE Transactions on Antennas and Propagation* 52, no. 2 (February 2004): 397–407. https://doi.org/10.1109/TAP.2004.823969.

[51] Reddy, J.N. *An Introduction to Nonlinear Finite Element Analysis*. Oxford University Press, 2004.

[52] "Overview of materials for Acrylonitrile Budadiene Styene (ABS.)" http://www.matweb.com/search/DataSheet.aspx?MatGUID=3a8afcddac864d4b8f58d40570d2e5aa&ckck=1. Web. Jan. 2020

[53] P.G. Lidquist, C. M. Wayman, Shape memory and transformtation behavior of martensitic Ti-Pd-Ni and Ti-Pt-Ni alloys, in: T.W. Duerig, K. N. Melton, D. Stöckel, C. M. Wayman (Eds.), Engineering Aspects of Shape Memory Alloys, Butterworth-Heinemann, London, 1990, pp. 58-68.

[54] Jasik, Henry, Richard C. Johnson. *Antenna Engineering Handbook*. McGraw-Hill, 1993.

[55] Silver, Samuel. *Microwave Antenna Theory and Design*. McGraw-Hill, 1949.

[56] Kastelic, Michael. "VHF Managers Handbook," July 2006.

[57] Yuan, X. "Three-Dimensional Electromagnetic Scattering from Inhomogeneous Objects by the Hybrid Moment and Finite Element Method." *IEEE Transactions on Microwave Theory and Techniques* 38, no. 8 (August 1990): 1053–58. https://doi.org/10.1109/22.57330.

[58] Botha, M.M., and J.-M. Jin. "On the Variational Formulation of Hybrid Finite Element-Boundary Integral Techniques for Electromagnetic Analysis." *IEEE Transactions on Antennas and Propagation* 52, no. 11 (November 2004): 3037–47. https://doi.org/10.1109/TAP.2004.835140.

[59] M. V. K. Chari, S. J. Salon, Numerical methods in electromagnetism, Academic Press, 2000.

[60] Elbeltagi, Emad, Tarek Hegazy, and Donald Grierson. "Comparison among Five Evolutionary-Based Optimization Algorithms." *Advanced Engineering Informatics* 19, no. 1 (January 2005): 43–53. https://doi.org/10.1016/j.aei.2005.01.004.

[61] Yildiz, Ali R. "Comparison of Evolutionary-Based Optimization Algorithms for Structural Design Optimization." *Engineering Applications of Artificial Intelligence* 26, no. 1 (January 2013): 327–33. https://doi.org/10.1016/j.engappai.2012.05.014.

[62] Nguyen, Anh-Tuan, Sigrid Reiter, Philippe Rigo, "A Review on Simulation-Based Optimization Methods Applied to Building Performance Analysis." *Applied Energy* 113, (September 2013): 1043-1058.

[63] Jones, Donald R, and Matthias Schonlau. “Efficient Global Optimization of Expensive Black-Box Functions.” *Journal of Global Optimization* 13, 1998: 455-492.

[64] Sacks, Jerome, William J. Welch, Toby J. Mitchell, Henry P. Wynn. “Design and Analysis of Computer Experiments.” *Statistical Science* 4, no. 4, (1989): 409-435.

[65] Baars, Jacob W.M. *The Paraboloidal Reflector Antenna in Radio Astronomy and Communication*. Springer, 2007.

[66] Balanis, Constantine A. *Antenna Theory Analysis and Design, Third Edition*. Wiley-Interscience, 2005.

[67] Altshuler, E. and Linden, D. “Wire-Antenna Designs Using Genetic Algorithms.” *IEEE Transactions on Antennas and Propagation* 39, No. 2 (April 1997): 33-43.

[68] Jape, Sameer, Milton Garza, Edwin Peraza Hernandez, Joshua Ruff, Francisco Espinal, Deanna Sessions, Gregory Huff, Dimitris C. Lagoudas, Darren J. Hartl. “Self-Folding Active Origami Reflector Antenna Enabled by Shape Memory Polymer Actuation.” *Smart Materials and Structures*, submitted 2020.